Frontiers | Frontiers in Earth Science

TYPE Original Research
PUBLISHED 07 November 2024
DOI 10.3389/feart.2024.1436573



OPEN ACCESS

EDITED BY
Hu Li,
Sichuan University of Science and Engineering, China

REVIEWED BY
Wendong Wang,
China University of Petroleum, China
Quanyou Liu,
SINOPEC Petroleum Exploration and Production Research Institute, China
Qianyou Wang,
University of Liverpool, United Kingdom

*CORRESPONDENCE
Maoyun Wang,
wmy950904@163.com
Jianhui Zeng,
zengjh@cup.edu.cn

RECEIVED 22 May 2024
ACCEPTED 28 October 2024
PUBLISHED 07 November 2024

CITATION
Wang M, Zeng J, Li C, Qiao J, Wei W, Zhang H and Cui H (2024) The impacts of $CO_2$ on sandstone reservoirs in different fluid environments: insights from mantle-derived $CO_2$ gas reservoirs in Dongying Sag, Bohai Bay Basin, China.
*Front. Earth Sci.* 12:1436573.
doi: 10.3389/feart.2024.1436573



# The impacts of $CO_2$ on sandstone reservoirs in different fluid environments: insights from mantle-derived $CO_2$ gas reservoirs in Dongying Sag, Bohai Bay Basin, China

Maoyun Wang[1,2]*, Jianhui Zeng[1,2]*, Chuanming Li[1,2], Juncheng Qiao[1,2], Wenfei Wei[1,2], Huanle Zhang[1,2] and Huwang Cui[1,2]

[1]National Key Laboratory of Petroleum Resources and Engineering, China University of Petroleum, Beijing, China, [2]College of Geosciences, China University of Petroleum, Beijing, China

**Introduction:** Mantle-derived $CO_2$, as an important component of hydrothermal fluids, is widely distributed in petroliferous basins. While previous experimental studies have suggested that $CO_2$ can improve sandstone reservoir quality through mineral dissolution in open fluid setting, they have overlooked its nagetive effects to sandstone reservoir quality by carbonate cementation. Additionally, the roles of various fluid environments in $CO_2$-reservoir interactions have not been studied in detail.

**Methods:** To systematically investigate the influences of $CO_2$ on sandstone reservoirs, we examine a typical mantle-derived $CO_2$ gas reservoir, Bohai Bay Basin, China. This study employs integrated methods, including electron microscopy, scanning electron microscopy, X-ray diffraction, stable C- and O-isotope analysis, and physical property data. The aim is to investigate the evidence and mechanisms by which mantle-derived $CO_2$ impacts sandstone reservoirs, particularly focusing on its effects in open and closed fluid environments.

**Results and Discussion:** Our findings reveal that dawsonite and ankerite are prevalent within the mantle-derived $CO_2$ gas reservoir, while isotopic analysis of carbonate cements indicates values ($\delta^{13}C$: −9.0‰ to −1.6‰; $\delta^{18}O$: −21.7‰ to −12.7‰) consistent with mantle-derived $CO_2$ and hydrothermal fluids. These pieces of evidence indicate that $CO_2$-rich hydrothermal fluids participate in water-rock interactions, thereby significantly influencing the diagenesis of reservoirs. Further, we notice that $CO_2$ reservoirs adjacent to faults exhibit an open fluid environment, characterized by superior porosity and permeability, more quartz, but fewer feldspar, carbonate, and clay minerals compared to those in closed fluid environments. Notably, kaolinite predominates in open fluid environments, while illite/smectite (I/S) is more common in closed settings. The dual roles of mantle-derived $CO_2$ are highlighted in our analysis: while it enhances reservoir storage and permeability through mineral dissolution, the carbonate cement generated by $CO_2$-water-rock interaction can also adversely affect reservoir quality. In open fluid environments, $CO_2$ facilitates the dissolution of feldspar and carbonate minerals, promoting the timely removal of dissolution by-products (clay mineral) and inhibiting carbonate cementation, thereby improving reservoir properties. Conversely, in closed fluid environments, decreasing $CO_2$ concentrations with depth leads to diminishing dissolution effects and increased carbonate cementation, resulting in reduced reservoir porosity and permeability. Overall, the significance of this study is to correct the deviation in the impacts of $CO_2$ on sandstone reservoirs at laboratory setting through case study of typical mantle-source $CO_2$ gas reservoir.

This work can be applied to the studies of reservoir homogeneity and sweet spots in regions with hydrothermal and mantle-derived $CO_2$ activities. However, due to the limitation of $CO_2$ content range (about 15%–70%) in the study case, we are unable to investigate the effects of low-concentration $CO_2$ on sandstone reservoirs, which may affect the generalizability of this work. Besides, the formation temperature and pressure, and salinity of formation water, should be considered when dealing with other cases.

KEYWORDS

**$CO_2$-water-rock interaction, fluid environment, mantle-derived $CO_2$, diagenesis, Dongying Sag**

## 1 Introduction

Hydrothermal activities have occurred in petroliferous basins during their formation and evolution (Zhang et al., 2023; Zhu et al., 2017). Mantle-derived $CO_2$, as a primary component of hydrothermal fluids (Diker et al., 2024; Liu et al., 2024; Ranta et al., 2023; Sun and Dasgupta, 2023), significantly influences reservoir quality, and hydrocarbon expulsion and migration (Dmitriyevskiy et al., 2010; Guo et al., 2011; Zhu, et al., 2017; Liu et al., 2017; Lu et al., 2022; Huang et al., 2021). Furthermore, basins with rift tectonic background frequently experience hydrothermal activities, leading to the development of $CO_2$-rich oil and gas fields, such as The South Atlantic Ocean margin (Anderson et al., 2023; Liu et al., 2022; Wright, 2020), Hailar (Yang et al., 2021; Liu et al., 2009), Songliao (Liu N. et al., 2019; Yang et al., 2009), Bohai Bay (Miao et al., 2020), Subei (Liu J. et al., 2023; Zhou et al., 2020; Liu et al., 2017), Sanshui (Zhu et al., 2017), Yinggehai (Liu Q. et al., 2019; Yang et al., 2023), and other rift basins in eastern China (Zhao et al., 2017). This mantle-derived $CO_2$ migrates into the reservoirs and dissolves in formation water, generating $H^+$ and $CO_3^{2-}$ (Li et al., 2015), where $H^+$ leads to the dissolution of aluminosilicate and carbonate minerals (Portier and Rochelle, 2005), while $CO_3^{2-}$ combines with ions like $Ca^{2+}$, $Mg^{2+}$, and $Fe^{2+}$ (Li et al., 2015), forming carbonate minerals that occupy pore space within the reservoirs. Therefore, in regions with hydrothermal activity, as well as high $CO_2$ concentrations, $CO_2$ is one of the critical factors that cannot be overlooked in contributing to reservoir heterogeneity. However, previous studies on mantle-derived $CO_2$ have mostly emphasized its positive effects on reservoirs (Liu Q. et al., 2023; Yuan et al., 2023; Liu et al., 2016; Zhou et al., 2020; Zhang et al., 2018), with little evidence showing its participation in carbonate cementation that could reduce reservoir quality (Hu, 2016). As a result, the overall impacts of mantle-derived $CO_2$ on reservoirs has not been comprehensively understood.

Most studies of $CO_2$-water-rock reaction experiments suggest that the dissolution of minerals by $CO_2$ does not always enhance reservoir porosity and permeability. In these experiments, the dissolution of feldspar and carbonate minerals by $CO_2$ increases the porosity of the core plugs (Wu et al., 2019; Fu et al., 2016; Yu et al., 2016; Fischer et al., 2010), while the permeability typically decreases as the pore throats are blocked by dissolution by-products, such as clay minerals (Pearce et al., 2019; Wu et al., 2019; Aminu et al., 2018). In the geological conditions, due to frequent fault activities in rift basins, reservoirs near faults often have relatively open fluid environments during geological history (Gudmundsson, 2022; Ward et al., 2016; Zhou et al., 2020; Wei et al., 2017; Li et al., 2016). The open fluid environments are conducive to the timely discharge of dissolution by-products, leading to significant improvements in reservoir porosity and permeability (Hu, 2016; Wei et al., 2017; Yuan et al., 2013a). However, most oil and gas reservoirs actually have a stable pressure system, and the fluid environment is relatively closed, making fluid migration and discharge of dissolution by-products relatively difficult (Yuan et al., 2013a; Zhao et al., 2016). Currently, there is a lack of systematic study on the impacts of mantle-derived $CO_2$ on reservoirs in different fluid environments, which, to some extent, limits the research on the reservoir homogeneity and the prediction of sweet spots in regions with hydrothermal activity, as well as high $CO_2$ concentrations.

Dongying Sag, located in Bohai Bay Basin, is characterized by numerous anticline oil and gas traps that have been modified by normal faults and are rich in mantle-derived $CO_2$ (Miao et al., 2020; Li et al., 2016). The mantle-derived $CO_2$ has unique stable carbon isotope compositions (Dai et al., 2001), which can contribute to confirming if the mantle-derived $CO_2$ participates in water-rock interactions and affects reservoirs (Liu R. et al., 2019; Hu, 2016; Liu et al., 2016). Therefore, Dongying Sag is an ideal place to research the synergistic impacts of fluid environments and $CO_2$ on reservoirs.

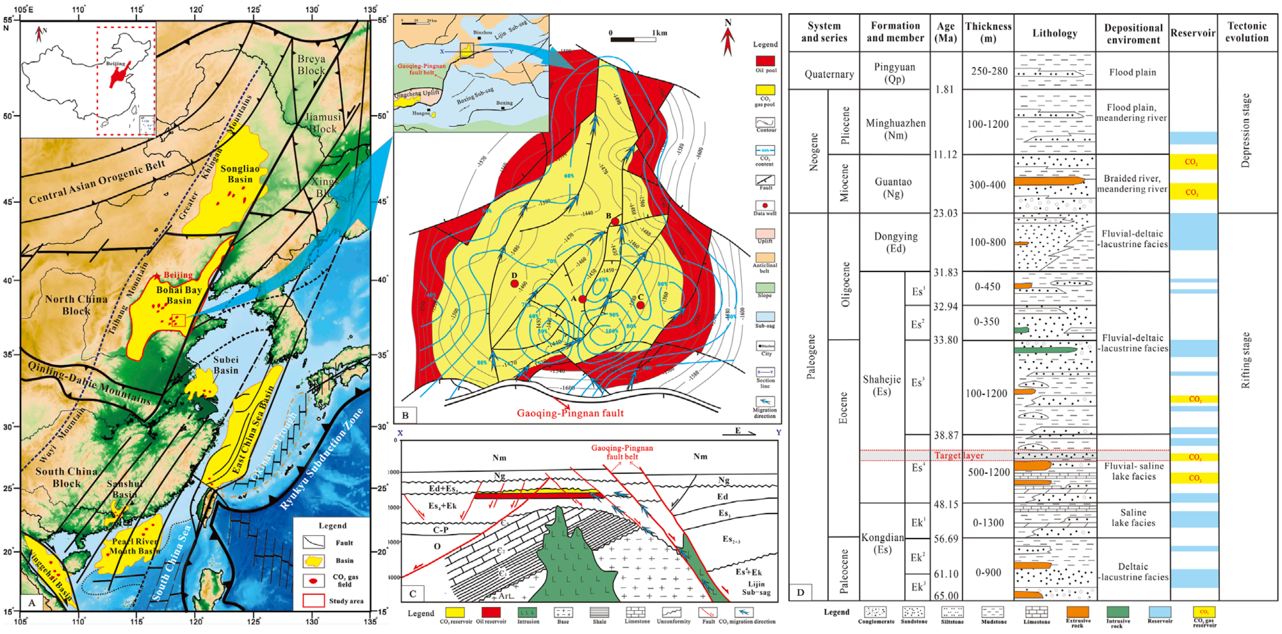


FIGURE 1
**(A)** Distribution of rift basins and $CO_2$ gas fields in eastern China [modified from Zhao et al. (2017)]. **(B)** Distribution of $CO_2$ gas fields in Dongying Sag, the top structure, $CO_2$ content distribution, and migration map of Pingfangwang $CO_2$ gas reservoir (modified from the Shengli Oilfield). **(C)** Profile map (see Figure 1B for location) and $CO_2$ source of study area (modified from Zeng, 2000). **(D)** Stratigraphy, lithology, tectonic movements, and reservoir distribution in the Dongying Sag [modified from Wei et al. (2017)].

This study examines typical mantle-derived $CO_2$ gas reservoirs in Dongying Sag as a case study, aiming to better understand the impacts of mantle-derived $CO_2$ on sandstone reservoirs in open and closed fluid environments using a multi-technique approach of combined mineralogy (Thin section, Scanning electron microscopy, and X-ray diffraction) and geochemistry (stable C- and O-isotopes). The main objectives of the current study are:

(1) To identify the mineralogical and geochemical evidence for the impacts of $CO_2$ on reservoirs.
(2) To investigate the characteristics of diagenetic minerals in mantle-derived $CO_2$ reservoirs and their impact on the sandstone reservoirs.
(3) To elucidate the impact mechanisms of $CO_2$ on sandstone reservoirs, with a focus on the impact laws of $CO_2$ on reservoirs in different fluid environments.

## 2 Geological setting

Due to the influence of the Pacific Plate's subduction, oil and gas fields rich in mantle-derived $CO_2$ are widely distributed in the rift basins of eastern China (Zhao et al., 2017) (Figure 1A). The Dongying Sag, located in the southeastern of the Bohai Bay Basin, is a graben of Mesozoic and Cenozoic (Niu et al., 2022). Along the Gaoqing-Pingnan deep fault in the Dongying Sag, there are several $CO_2$ gas fields (Han et al., 2010) (Figure 1B). These $CO_2$ mainly migrate from the mantle to sedimentary basins through magmatic activity and deep faults (Figure 1C) (Zhang et al., 2023; Guo et al., 2006), have special stable carbon isotope compositions (with $\delta^{13}C$ mostly around −6‰ ± 2‰) (Dai et al., 2001).

Since the Cenozoic, the Gaoqing-Pingnan deep fault has been active, accompanied by multiple magmatic and mantle-derived $CO_2$ activity events, forming multiple sets of $CO_2$-rich reservoirs (Figure 1D) (Kang et al., 2014; Cheng et al., 2020). According to drilling data, the Cenozoic stratigraphic unit includes the Kongdian Formation (Ek), Shahejie Formation (Es), Dongying Formation (Ed), Guantao Formation (Ng), Minghuazhen Formation (Nm), and Pingyuan Formation (Qp) (Figure 1D). Sediments of the Cenozoic strata in the Dongying Sag include the saline lake-delta-fluvial (the rifting stage) and fluvial (the depression stage) (Niu et al., 2022).

Pingfangwang $CO_2$ gas field, the typical mantle-derived $CO_2$ gas reservoir selected in this study, is an anticlinal trap that has been reformed by normal faults (Figure 1B). The target layer is a set of beach-bar sand in the 4th member of Shahejie Formation ($Es^4$) (Figure 1D). Its natural gas is mainly composed of $CO_2$, with a content of 61.2%–98.6%, $CO_2$ content decreases from south to north (Figure 1B). The $\delta^{13}C_{CO2}$ ranges from −5.08‰–−4.32‰. $CO_2$ from the mantle first migrates vertically to the target layer through the Gaoqing-Pingnan deep fault and then migrates northward through some nearly south-north trend normal faults (Figures 1B, C) (Wang et al., 2004; Zeng, 2000).

## 3 Data and methods

To investigate the characteristics of mantle-derived $CO_2$ reservoirs in the study area, 1,343 sets of porosity and permeability data and 46 sandstone samples of target layers from 4 wells (represented as red circles in Figure 1B) were collected from the PEDRI, Shengli Oilfield. Four types of experiments were performed on these sandstone samples. 21 casting thin sections were observed using an optical microscope. Selected typical samples underwent scanning electron microscopy. X-ray diffraction analysis was conducted on 15 groups for whole rock and clay minerals. Additionally, C and O isotope analysis was carried out on a total of 10 sandstone samples and carbonate veins.

## 3.1 Analysis of thin sections

Thin sections were impregnated with blue epoxy resin to highlight the pore space and were dyed with Alizarin Red-S and K-ferricyanide for carbonate mineral identification. Calcite was dyed red, ferrocalcite was dyed purplish red, and ankerite was dyed blue-purple. Thin sections were observed using the Leica 4500P polarizing microscope. ImageJ software was used for quantitative analysis of surface porosity.

## 3.2 Scanning electron microscopy (SEM)

The Quanta-200F SEM was used to observe the fresh surface of gold-plated rock samples, facilitating the identification of diagenetic phenomena and minerals. The SEM was operated at an acceleration voltage of 20 kV and an emission current of 3 nA.

## 3.3 Whole rock and clay X-ray diffraction analysis (XRD)

Each group of samples was crushed and mixed evenly. A portion of the powder was used for whole rock XRD analysis, while the remainder was analyzed for clay XRD. This approach was adopted to minimize the effect of lithologic heterogeneity. The D8 Advance X-ray diffractometer was used for whole rock and clay X-ray diffraction analysis. This allowed for quantitative analysis of the types and contents of the whole rock and clay minerals in $CO_2$ reservoirs.

## 3.4 Stable C- and O-isotope analysis

Eight whole rocks and two calcite vein samples were selected for C- and O-isotope analysis. A ThermoFisher MAT-253 stable isotope mass spectrometer was used to determine the $\delta^{13}C$ and $\delta^{18}O$ of carbonate cement.

## 3.5 Calculation of carbonate cement formation temperature

To confirm the correlation between carbonate minerals in $CO_2$ reservoirs and mantle-derived $CO_2$ with high crystallization temperature properties, we calculated the precipitation temperatures of carbonate minerals in mantle-derived $CO_2$ gas reservoirs using the Formula 1 established by Friedman and O'Neil (1977).

$$1000 * \ln \alpha_{carbonate-water} \approx \delta^{18}O_{carbonate} - \delta^{18}O_{water} = 2.78 * 10^6/T^2 - 2.89 \quad (1)$$

Where $\alpha_{carbonate-water}$ is the fractionation coefficient, $\delta^{18}O_{carbonate}$ is the $\delta^{18}O_{PDB}$ value of carbonate, The $\delta^{18}O_{V\text{-}SMOW}$ value of pore water in the study area is −2.55‰ (Han et al., 2012), T is the temperature of carbonate precipitation.

# 4 Results

## 4.1 Petrology characteristics and mineral compositions of $CO_2$ gas reservoirs

The identification results from the thin sections (Table 1) show that the terrigenous detrital components of $CO_2$ reservoirs consist of quartz (average: 73.0%, range: 58.8%–86.8%), feldspars (average: 13.4%, range: 3.8%–23.7%), and rock fragments (average: 13.7%, range: 4.6%–24.3%). There is a significant difference between the reservoirs near the faults (wells A and B) and the reservoirs far away from the faults (wells C and D). The former has a higher quartz content and a lower feldspar content, with the lithology consisting of feldspathic litharenite and sublitharenite (Li et al., 2024), while the latter mainly consists of lithic arkose (Figure 2).

The XRD results for whole rock and clay minerals (Table 2) show that the mineral composition of the $CO_2$ sandstone reservoir in the study area is predominantly quartz, with an average of 58.2%, with a relatively low content of feldspar (K-feldspar and plagioclase). Moreover, carbonate minerals are widely developed, comprising an average content of 12.6% calcite, 6.0% ankerite, 3.1% dawsonite, and small amounts of siderite. Among them, Wells A, B, C, and D have average quartz contents of 69.8%, 67.1%, 47.3%, and 45.5%, respectively. The average contents of total carbonate minerals (calcite, ankerite, siderite, and dawsonite) are 10.2%, 11.6%, 36.6%, and 40.3%, respectively. The average contents of clay minerals are 7.1%, 6.9%, 9.0%, and 12.4%, respectively. As for clay minerals, kaolinite dominates with an average of 40.9%, followed by the illite/smectite (I/S) mixed layer, with an average of 35.3%. Among them, the average relative content of kaolinite in Wells A, B, C and D are 52%, 58%, 23%, and 27%, respectively, and the average relative content of I/S is 28%, 21%, 52%, and 42%, respectively.

The mineral composition exhibits a noticeable contrast between reservoirs near and far from faults (Figure 3). The former displays higher quartz content and lower content of calcite, ankerite, and clay minerals compared to the latter. Furthermore, the clay minerals in the reservoirs near faults are predominantly kaolinite, whereas these in the reservoirs far from the faults primarily consist of I/S.

## 4.2 Porosity and permeability of $CO_2$ gas reservoirs

According to the statistical results of porosity and permeability data (Figure 4), The porosity of $CO_2$ reservoirs is concentrated

TABLE 1 Thin section identification results of $CO_2$ gas reservoirs in the study area.

| Location | Well | Depth(m) | The detrital grain volume fraction | | | Surface porosity | | | Ratio of DSP (%) |
|---|---|---|---|---|---|---|---|---|---|
| | | | Quartz (%) | Feldspar (%) | Rock fragment (%) | PSP (%) | DSP (%) | TSP (%) | |
| Near faults | A | 1,464.80 | 86.4 | 8.6 | 4.9 | 6.8 | 20.5 | 27.3 | 75.1 |
| | A | 1,496.90 | 76.9 | 3.8 | 19.3 | 9.2 | 26.0 | 35.2 | 73.9 |
| | A | 1,531.49 | 85.2 | 9.3 | 5.6 | 6.5 | 25.0 | 31.5 | 79.4 |
| | A | 1,557.11 | 86.8 | 6.6 | 6.6 | 7.4 | 22.0 | 29.4 | 74.8 |
| | A | 1,582.64 | 71.4 | 11.9 | 16.7 | 6.1 | 20.0 | 26.1 | 76.6 |
| | Means of Well A | | 81.4 | 8.0 | 10.6 | 7.2 | 22.7 | 29.9 | 76.0 |
| | B | 1,442.00 | 76.4 | 9.9 | 13.7 | 4.4 | 18.0 | 22.4 | 80.4 |
| | B | 1,457.00 | 86.5 | 5.6 | 7.8 | 5.6 | 20.0 | 25.6 | 78.0 |
| | B | 1,472.26 | 73.3 | 10.0 | 16.7 | 6.0 | 16.0 | 22.0 | 72.7 |
| | B | 1,496.90 | 70.6 | 9.6 | 19.8 | 8.5 | 18.4 | 26.9 | 68.5 |
| | B | 1,518.70 | 69.8 | 12.9 | 17.3 | 5.9 | 16.3 | 22.2 | 73.4 |
| | B | 1,537.62 | 66.3 | 14.1 | 19.6 | 7.8 | 13.8 | 21.6 | 63.9 |
| | Means of Well B | | 73.8 | 10.4 | 15.8 | 6.4 | 17.1 | 23.5 | 72.8 |
| Far from faults | C | 1,503.00 | 75.4 | 20.0 | 4.6 | 6.0 | 16.4 | 22.4 | 73.2 |
| | C | 1,527.90 | 72.2 | 13.9 | 13.9 | 4.9 | 11.5 | 16.4 | 70.1 |
| | C | 1,543.40 | 65.7 | 10.0 | 24.3 | 6.6 | 6.0 | 12.6 | 47.6 |
| | C | 1,569.96 | 63.2 | 23.7 | 13.2 | 1.3 | 7.0 | 8.3 | 84.3 |
| | C | 1,626.80 | 58.8 | 23.5 | 17.6 | 0.0 | 4.2 | 4.2 | 100.0 |
| | Means of Well C | | 67.1 | 18.2 | 14.7 | 3.8 | 9.0 | 12.8 | 75.1 |
| | D | 1,460.23 | 75.0 | 18.8 | 6.3 | 7.7 | 19.1 | 26.8 | 71.3 |
| | D | 1,495.30 | 75.0 | 12.5 | 12.5 | 6.0 | 12.5 | 18.5 | 67.6 |
| | D | 1,512.80 | 67.9 | 16.7 | 15.4 | 6.6 | 8.0 | 14.6 | 54.8 |
| | D | 1,530.45 | 64.9 | 15.6 | 19.5 | 5.9 | 5.0 | 10.9 | 45.9 |
| | D | 1,556.30 | 64.7 | 23.5 | 11.8 | 4.5 | 4.0 | 8.5 | 47.1 |
| | Means of Well D | | 69.5 | 17.4 | 13.1 | 6.1 | 9.7 | 15.9 | 57.3 |
| Means | | | 73.0 | 13.4 | 13.7 | 5.9 | 14.7 | 20.6 | 70.4 |

Abbreviation: Q–quartz; F–feldspar; RF–rock fragment; PSP–primary surface porosity; DSP–dissolution surface porosity; TSP–total surface porosity.

between 20% and 30% (Figure 4A), with an average of 23.6%. The permeability of $CO_2$ reservoirs near faults is mainly distributed in the range of 10 ~ 1,000 mD, with an average of 131.7 mD, while $CO_2$ reservoirs far from faults have permeability mainly distributed in the range of 1 ~ 100 mD, with an average of 24.3 mD (Figure 4B). As a whole, the physical properties of reservoirs near faults is better than that far from faults (Figure 4). The linear correlations between the porosity and permeability of $CO_2$ reservoirs are fair (Figure 4C),

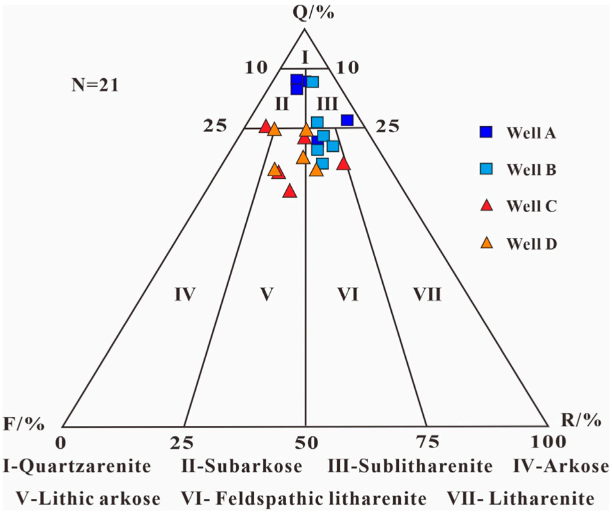


FIGURE 2
Detrital grain composition triangle diagram in the $CO_2$ gas reservoirs [revised from Folk (1968)]. Well A and B are near the faults, while well C and D are far from the faults. Q, Quartz; F, Feldspar; R, Rock fragment.

suggesting that the pores are the main seepage channels in $CO_2$ reservoirs.

## 4.3 Typical diagenesis in $CO_2$ gas reservoirs

### 4.3.1 Carbonate mineral cementation

Carbonate cementation is the predominant cementation process of $CO_2$ reservoirs in the study area, mainly developing dawsonite (Figures 5A–C), calcite (Figures 5C–F), ankerite (Figures 5C, F, G), and a small amount of siderite (Figures 5D, H) and dolomite (Figure 5I).

#### 4.3.1.1 Dawsonite

Dawsonite, a special carbonate mineral, can stably exist in high-concentration $CO_2$ environments. It is generated by the continuous reaction of K-feldspar, plagioclase, or kaolinite with $CO_2$ and the formation water (Ryzhenko, 2006; Johnson et al., 2011). Observation of thin sections and SEM confirms that all $CO_2$ gas reservoirs have dawsonite, with extremely high recognition. It is filled in the pores of sandstone, forming a hairlike or radial aggregate with a size of approximately 100–200 μm (Figures 5A–C).

#### 4.3.1.2 Calcite

Calcite is the most carbonate mineral in $CO_2$ reservoirs (Table 1), with pack-pore cementation (Figure 5C) or filling dissolution pores (Figure 5D). It frequently coexists with kaolinite (Figure 5E), indicating that these calcites formed after $CO_2$ injection into the reservoir. The coexistence of kaolinite and calcite is due to the acidic environment generated by $CO_2$, which causes feldspar to dissolve and form kaolinite. Later, the geological environment changes to alkaline, allowing calcite to precipitate within the pre-existing dissolution pores. Notably, some dissolution pores have not yet been incompletely filled (Figure 5D).

#### 4.3.1.3 Ankerite

Ankerite is commonly developed in $CO_2$ reservoirs, filling dissolution pores and intergranular pores (Figures 5C, F, G). Some ankerites replaced calcite (Figure 5F), indicating that the formation time of ankerite was later than that of calcite.

#### 4.3.1.4 Siderite and dolomite

Additionally, the $CO_2$ reservoir contains minor amounts of authigenic siderite (Figures 5D, H) and dolomite (Figure 5I). The dolomite was only observed under the microscope but not detected in the whole rock XRD analysis (Table 2).

### 4.3.2 Dissolution

The $CO_2$ reservoir in the study area exhibits intensive dissolution of feldspars, rock fragments, and calcites, forming numerous dissolution pores (Figure 5J–L). Remarkably, certain feldspar particles and calcite have undergone near-complete dissolution, forming mold pores (Figures 5J, K). Although some of the dissolution products, such as kaolinite and authigenic quartz, are filled in the dissolution pores (Figure 5L), and the carbonate minerals in the later stage are partially or completely filled in the dissolution pores (Figures 5C–E), the identification results of $CO_2$ reservoir thin sections show that the dissolution pores in the $CO_2$ reservoir still occupy an absolutely dominant position, with an average dissolution surface porosity of 14.7% and an average proportion of 70.4% (Table 1). In addition, the average dissolution porosity in the reservoirs near the faults is 19.4%, while the average dissolution porosity of reservoirs far from the faults is 9.4%. Obviously, the former is much greater than the latter.

## 4.4 The characteristics of carbon and oxygen isotopes in $CO_2$ gas reservoirs

Analysis results from carbonate veins and whole rock carbon and oxygen isotopes (Table 3) show that the $\delta^{13}C$ of carbonate minerals in mantle-derived $CO_2$ gas reservoirs are −9.0‰–−1.6‰, with an average of −5.2‰, and the $\delta^{18}O$ are −21.7‰–−12.7‰, with an average of −17.0‰. The average precipitation temperature of carbonate minerals in the study area was 121.9°C, which is much higher than the formation temperature.

# 5 Discussions

## 5.1 Evidence of the impact of mantle-derived $CO_2$ on reservoirs

$CO_2$ from the mantle has a unique range of C- and O-isotopes and high-temperature properties of mantle-derived fluids (e.g., Morishita, 2023; Ewa et al., 2012; Jin et al., 2013; Hou et al., 2019), and following prolonged interactions with the formation water and rocks, it ultimately generates carbonate minerals (e.g., Johnson et al., 2011; Harrison et al., 2019; Wei, et al., 2023). Thus, the impact of $CO_2$ on reservoirs can be confirmed based on the carbonate minerals generated during the mantle-derived $CO_2$-water-rock interactions and their isotopic characteristics.

10.3389/feart.2024.1436573

TABLE 2 Whole rock and clay X-ray diffraction analysis results of $CO_2$ gas reservoirs in the study area.

| Well | | Depth (m) | Content of whole-rock minerals (%) | | | | | | | | Relative content of clay minerals (%) | | | | |
|---|---|---|---|---|---|---|---|---|---|---|---|---|---|---|---|
| | | | Quartz | K-feldspar | Plagioclas | Calcite | Ankerite | Siderite | Dawsonite | TCCM | I/S | I | K | C | Ratio of I/S |
| Near faults | A | 1,464.80 | 81.5 | 8.7 | 0.0 | 0.0 | 1.0 | 0.0 | 0.2 | 7.1 | 26 | 11 | 59 | 4 | 45 |
| | A | 1,496.90 | 70.6 | 10.2 | 0.0 | 5.6 | 1.6 | 1.3 | 4.7 | 6.0 | 24 | 16 | 48 | 12 | 50 |
| | A | 1,531.49 | 64.4 | 7.2 | 5.7 | 3.3 | 1.7 | 1.1 | 8.5 | 8.1 | 30 | 11 | 52 | 7 | 40 |
| | A | 1,557.11 | 62.6 | 9.8 | 8.8 | 8.0 | 2.9 | 0.7 | 0.0 | 7.2 | 32 | 15 | 49 | 4 | 35 |
| | Means of Well A | | 69.8 | 9.0 | 3.6 | 4.2 | 1.8 | 0.8 | 3.4 | 7.1 | 28 | 13 | 52 | 7 | 43 |
| | B | 1,442.00 | 62.3 | 9.4 | 7.4 | 6.8 | 1.0 | 0.9 | 4.1 | 8.1 | 32 | 15 | 46 | 7 | 50 |
| | B | 1,457.00 | 75.0 | 8.2 | 8.0 | 3.8 | 0.8 | 0.0 | 0.0 | 4.2 | 8 | 6 | 82 | 4 | 55 |
| | B | 1,496.90 | 71.1 | 5.1 | 9.5 | 5.9 | 1.8 | 0.0 | 0.0 | 6.6 | 19 | 14 | 57 | 10 | 35 |
| | B | 1,537.62 | 60.1 | 6.4 | 3.6 | 10.4 | 7.7 | 0.4 | 2.9 | 8.5 | 24 | 19 | 48 | 9 | 50 |
| | Means of Well B | | 67.1 | 7.3 | 7.1 | 6.7 | 2.8 | 0.3 | 1.8 | 6.9 | 21 | 14 | 58 | 8 | 48 |
| Far from faults | C | 1,503.00 | 67.1 | 8.7 | 0.9 | 6.3 | 4.3 | 0.9 | 3.4 | 8.4 | 63 | 10 | 15 | 12 | 50 |
| | C | 1,527.90 | 56.3 | 8.4 | 1.2 | 15.8 | 4.6 | 0.3 | 3.5 | 9.9 | 43 | 14 | 38 | 5 | 45 |
| | C | 1,569.96 | 21.8 | 2.5 | 0.0 | 9.8 | 50.8 | 1.3 | 6.6 | 7.2 | 52 | 22 | 23 | 3 | 55 |
| | C | 1,626.80 | 43.8 | 6.7 | 0.0 | 35.1 | 3.8 | 0.0 | 0.0 | 10.6 | 50 | 20 | 14 | 16 | 55 |
| | Means of Well C | | 47.3 | 6.6 | 0.5 | 16.8 | 15.9 | 0.6 | 3.4 | 9.0 | 52 | 17 | 23 | 9 | 51 |
| | D | 1,512.80 | 57.8 | 7.6 | 1.3 | 11.6 | 5.4 | 0.6 | 3.2 | 12.5 | 43 | 25 | 19 | 13 | 45 |
| | D | 1,530.45 | 34.7 | 7.4 | 1.1 | 26.8 | 3.2 | 2.3 | 10.0 | 14.5 | 39 | 23 | 30 | 8 | 45 |
| | D | 1,556.30 | 44.1 | 5.4 | 0.0 | 40.3 | 0.0 | 0.0 | 0.0 | 10.2 | 44 | 17 | 33 | 6 | 55 |
| | Means of Well D | | 45.5 | 6.8 | 0.8 | 26.2 | 2.9 | 1.0 | 4.4 | 12.4 | 42 | 22 | 27 | 9 | 48 |
| Means | | | 58.2 | 7.4 | 3.2 | 12.6 | 6.0 | 0.7 | 3.1 | 8.6 | 35.3 | 15.9 | 40.9 | 8.0 | 47.3 |

Abbreviation: TCCM–total content of clay minerals, I/S–illite and smectite mixed layer, I–illite, K–kaolinite, C–chlorite.

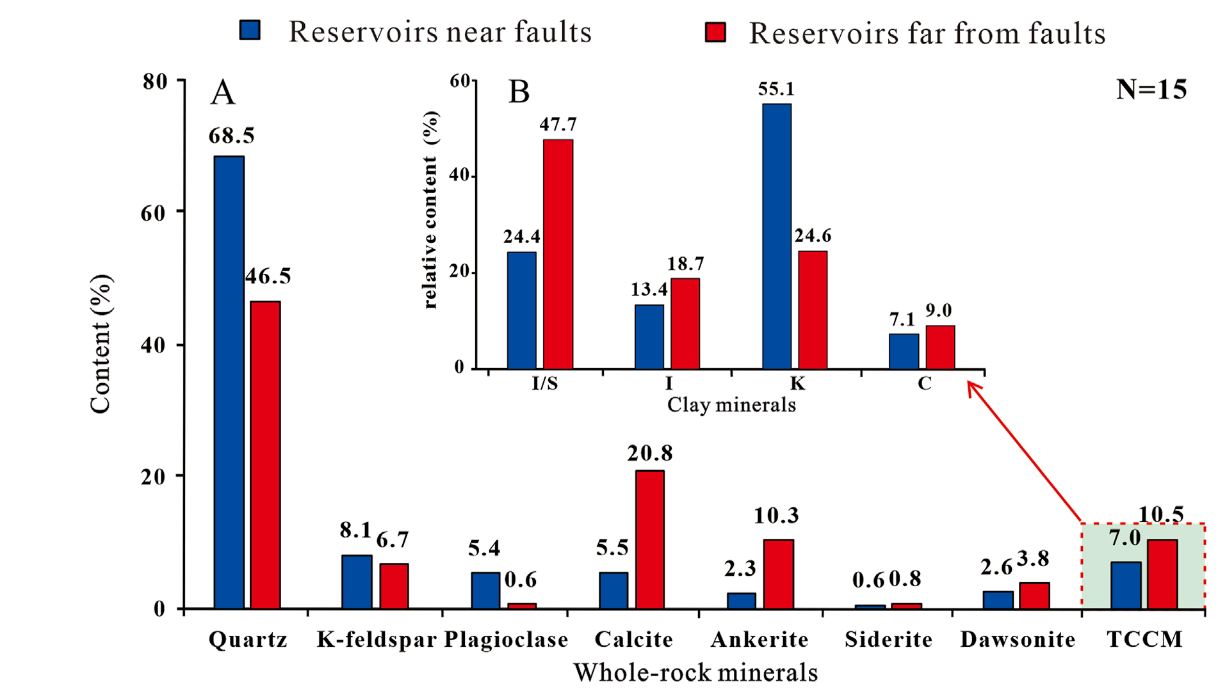


FIGURE 3
Mineral compositions of $CO_2$ gas reservoirs near and far from faults in the study area. **(A)** Histogram of mineral whole-rock content. **(B)** Histogram of relative content of clay minerals. TCCM–total contents of clay minerals.

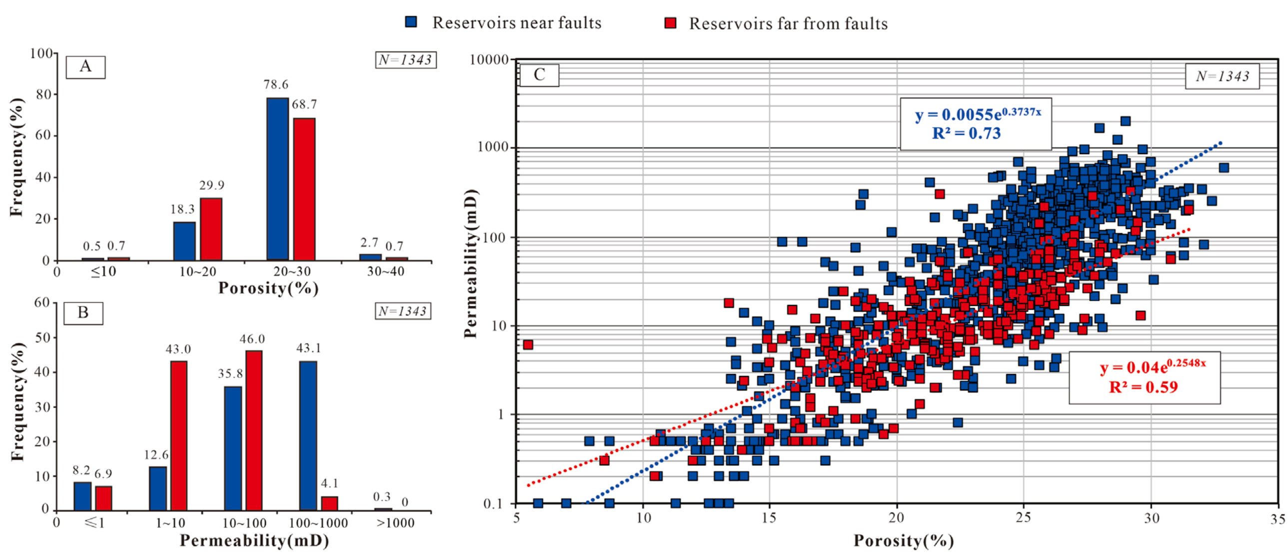


FIGURE 4
Characteristics of porosity and permeability of reservoirs near and far from faults. **(A)** Histogram of porosity frequency distribution. **(B)** Histogram of permeability frequency distribution. **(C)** The relationship of porosity and permeability in the $CO_2$ gas reservoirs.

### 5.1.1 Evidence from carbonate minerals

Dawsonite is the product of the long-term reaction between high-concentration mantle-derived $CO_2$ and formation water, as well as various feldspar (Equations 2–4), and is considered a "tracer mineral" for mantle-derived $CO_2$ fluid migration and accumulation (Ryzhenko, 2006; Liu et al., 2009; Johnson et al.,

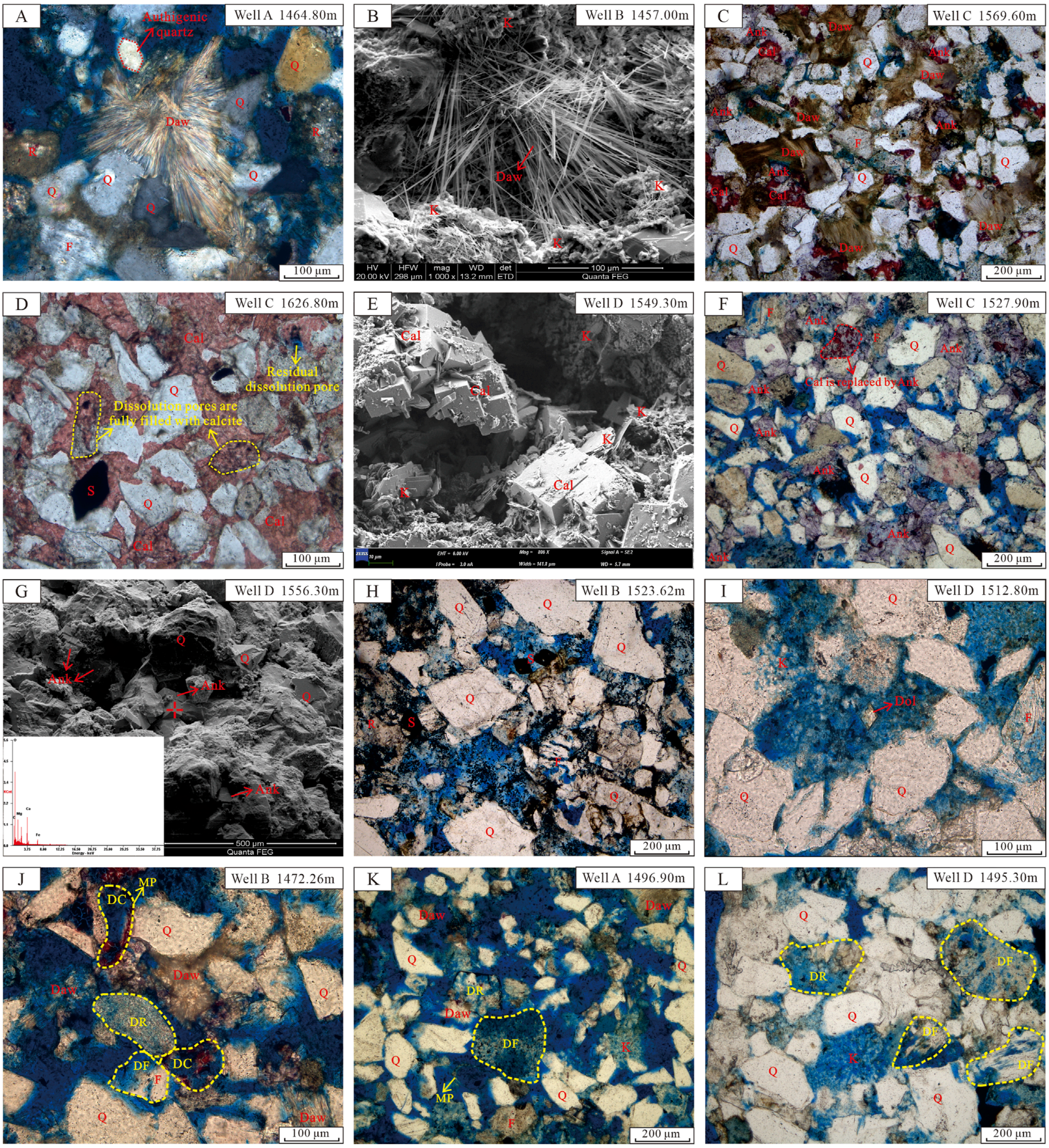

FIGURE 5
Pictures of carbonate cements and dissolution in $CO_2$ reservoirs. Picture **(A)** is derived from observations under cross-polarized light. Pictures **(B, E, G)** are derived from observations under SEM. Pictures **(C, D, F)**, and H-L are derived from observations under single polarized light. **(A)** Dawsonite accompanied with authigenic quartz **(B)** Dawsonite; **(C)** Dawsonite, calcite (dyed red) and ankerite (dyed blue-purple) cement; **(D)** calcite cement (dyed red), dissolution pores filled with calcites and unfilled residual dissolution pore; **(E)** Paragenesis of calcite and kaolinite; **(F)** Ankerite and calcite replaced by ankerite; **(G)** Ankerite and its energy dispersive spectrum analysis results **(H)** Rhombic authigenic siderite; **(I)** Authigenic dolomite; **(J)** Coexistence of dawsonite cement and intensive dissolution (feldspar, rock fragment, and calcite); **(K)** Coexistence of dawsonite, kaolinite and intensive dissolution (feldspar and rock fragment), some particles are completely dissolved and formed mold holes; **(L)** Coexistence of kaolinite and obvious dissolution (feldspar and rock fragment). Q, quartz; F, feldspar; R, rock fragment; Daw, dawsonite; Cal, calcite; Ank, ankerite; S, siderite; K, kaolinite; DR, dissolution of rock fragment; DF, dissolution of feldspar; DC, dissolution of calcite; MP, mold pore.

TABLE 3 The carbon and oxygen isotope data of whole rock and veins and the precipitation temperature of carbonate minerals of $CO_2$ gas reservoirs.

| Well | Depth (m) | Sample types | $\delta^{13}C_{PDB}$(‰) | $\delta^{18}O_{PDB}$(‰) | FT (°C) | CPT (°C) |
|---|---|---|---|---|---|---|
| A | 1,496.90 | Whole rock | −6.4 | −17.6 | 76.9 | 124.5 |
| A | 1,557.11 | Vein | −8.0 | −19.3 | 79.2 | 145.3 |
| B | 1,442.00 | Vein | −4.8 | −12.7 | 74.8 | 78.5 |
| B | 1,457.00 | Whole rock | −1.7 | −16.2 | 75.4 | 109.6 |
| B | 1,537.62 | Whole rock | −4.2 | −19.3 | 78.4 | 145.3 |
| C | 1,527.90 | Whole rock | −5.0 | −13.7 | 78.1 | 86.6 |
| C | 1,569.96 | Whole rock | −1.6 | −16.3 | 79.7 | 110.6 |
| C | 1,626.80 | Whole rock | −6.6 | −19.4 | 81.8 | 146.6 |
| D | 1,530.45 | Whole rock | −5.0 | −14.2 | 78.2 | 90.9 |
| D | 1,556.30 | Whole rock | −9.0 | −21.7 | 79.1 | 181.0 |
| Mean | | | −5.2 | −17.0 | 78.1 | 121.9 |

Abbreviation: GT, formation temperature; CPT, carbonate precipitation temperature.

2011). In the study area, dawsonite cement is generally developed (Figures 5A–C, J, K), while only a small amount of plagioclase and K-feldspar are present (Table 2), suggesting that the reaction between feldspar and mantle-derived $CO_2$ has generated dawsonite.

$$KAlSi_3O_{8(K-feldspar)} + Na^+ + CO_2 + H_2O \rightarrow NaAlCO_3(OH)_{2(Dawsonite)} + 3SiO_{2(Quartz)} + K^+ \quad (2)$$

$$NaAlSi_3O_{8(Albite)} + CO_2 + H_2O \rightarrow NaAlCO_3(OH)_{2(Dawsonite)} + 3SiO_{2(Quartz)} \quad (3)$$

$$CaAl_2Si_2O_{8(Anorthite)} + 2Na^+ + 3CO_2 + 3H_2O \rightarrow 2NaAlCO_3(OH)_{2(Dawsonite)} + CaCO_{3(Calcite)} + SiO_{2(Quartz)} + 2H^+ \quad (4)$$

Moreover, ankerite is generally considered a kind of cement in the middle to late diagenetic stage (e.g., Oluwadebi et al., 2018; Ma et al., 2018; Han et al., 2012), with a high precipitation temperature, and the precipitation temperatures of ankerite in Dongying Sag are about 110°C–135°C (Han et al., 2012). The ratio of I/S in mantle source $CO_2$ reservoirs is mainly between 40% and 55% (Table 2), indicating that the current diagenetic evolution is still in the early to middle diagenetic stage. However, the theoretical burial temperature of $CO_2$ reservoirs is 74.8°C–81.8°C in the study area (Table 3) (Gong et al., 2013), which is much lower than the precipitation temperature of ankerite. That is to say, the formation of ankerite (Figures 5C, F, G) occurs in a high-temperature environment formed by hydrothermal fluids rich in $CO_2$. And there is a close genetic relationship between ankerite and mantle-derived $CO_2$ in the study area.

### 5.1.2 Evidence from carbon and oxygen isotopes

According to the results of C- and O-isotopes analysis (Table 3), the $\delta^{13}C$ values of carbonate minerals in the mantle-derived $CO_2$ reservoir range from −9.0‰–−1.6‰, with an average of −5.2‰. Which basically fall within the range suggested for mantle-derived $CO_2$ (−8‰–4‰VPDB; Morishita, 2023; Dai et al., 2001). Moreover, the precipitation temperature of carbonate minerals is generally much higher than the maximum theoretical formation temperature (Table 3). Furthermore, the carbon and oxygen isotope data were submitted to the genetic chart of carbonate cement in the Bohai Bay Basin established by (Wang and Zhang, 2001), which showed that carbonate cement in mantle-derived $CO_2$ reservoirs was mainly formed in a transitional environment of low-temperature hydrothermal and high-temperature magmatic-hydrothermal fluids (Figure 6; e.g., Hou et al., 2019).

In summary, evidence from minerals and carbon and oxygen isotopes suggests that mantle-derived $CO_2$ indeed interacts with formation water and rocks, ultimately generating diverse carbonate cements precipitated in fractures and pores.

## 5.2 The dual effects of mantle-derived $CO_2$ on sandstone reservoirs

The mechanism of the impact of $CO_2$ on reservoirs by previous studys mainly comes from $CO_2$-water-rock reaction experiments. In these experiments, $CO_2$ fluids were injected into core plugs to make $CO_2$, water, and rock to fully react. And the porosity, permeability, and mineral changes of core plugs were measured pre- and post-experiment (e.g., Fischer et al., 2010; Aminu et al., 2018; Pearce et al., 2019; Wu et al., 2019; Fu et al., 2016). These studies generally indicate that dissolution is the main reaction between $CO_2$ and rocks, resulting in an increase in porosity (Wu et al.,

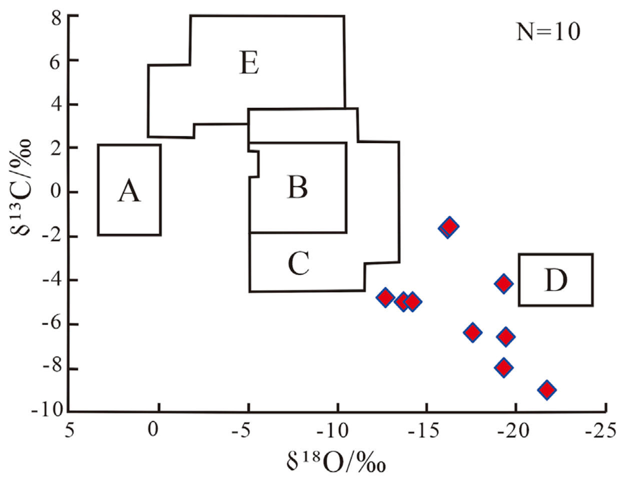


FIGURE 6
Origin of carbonate minerals (veins and cement) of mantle-derived $CO_2$ reservoirs in the study area [modified from Wang and Zhang (2001)]. A–carbonates sediment in low salinity solution. B–carbonate sediment in seawater salinity solution. C–carbonate sediment of cryogenic hydrothermal origin. D–carbonate sediment of magmatic-hydrothermal origin. E–carbonate sediment of lacustrine.

2019; Fu et al., 2016; Yu et al., 2016; Fischer et al., 2010) and a decrease in permeability due to blockage of throats by by-products of dissolution (Pearce et al., 2019; Wu et al., 2019; Aminu et al., 2018). However, the open fluid environment in the formation is relatively limited and generally found near faults (Zhou et al., 2020; Wei et al., 2017). On the contrary, most oil and gas reservoirs feature relatively closed fluid environments, making fluid migration relatively difficult (Yuan et al., 2013a; Zhao et al., 2016). Additionally, various ions can also participate in the water-rock reactions (Ahmat et al., 2022; Portier and Rochelle, 2005; Li et al., 2015). Therefore, the previous works cannot fully elucidate the impact of $CO_2$ on reservoirs.

In the high-temperature and high-pressure environment of the formation, the $CO_2$-water-rock reaction theoretically has dual effects on the sandstone reservoirs (Portier and Rochelle, 2005; Li et al., 2015). On the one hand, A large amount of $CO_2$ dissolves in the formation water and forms weak acids ($H^+$) (Equation 5), which then dissolve the carbonate minerals and aluminosilicate minerals, such as K-feldspar, plagioclase, and so on (Portier and Rochelle, 2005). On the other hand, the $CO_3{}^{2-}$ formed in (Equation 5) combines with $Ca^{2+}$, $Mg^{2+}$, and $Fe^{2+}$ in the formation water to generate stable carbonate minerals (Equation 6; Li et al., 2015).

$$CO_2 + H_2O \rightarrow CO_3^{2-} + 2H^+ \qquad (5)$$

$$(Ca, Mg, Fe)^{2+} + CO_3^{2-} \rightarrow (Ca, Mg, Fe)\,CO_{3\,(\text{Carbonates minerals})} \qquad (6)$$

### 5.2.1 The impacts of dissolution by mantle-derived $CO_2$ on reservoirs

During the diagenetic evolution of reservoirs, dissolution is the key factor for good physical properties of oil and gas reservoirs (Ehrenberg and Baek, 2019). The dissolution in the mantle-derived $CO_2$ reservoirs is extremely strong (e.g., Liu N. et al., 2023; Liu et al., 2016; Zhou et al., 2020). The intensive dissolution of feldspars, rock fragments, and calcites forms a large number of dissolution pores (Figure 5J–L), and even some feldspar and calcite almost completely dissolved to form mold pores (Figures 5J, K). As a result, the dissolution pores occupy the absolute dominant position in the pore system of the study area (Table 1). Therefore, the dissolution of feldspar and early calcite by $CO_2$ in the study area greatly increases the storage space for oil and gas, and simultaneously, the seepage channels are also improved (Figure 4). Mantle-derived $CO_2$ plays a crucial role in improving the physical properties of reservoirs in the study area.

### 5.2.2 The impacts of cementation by mantle-derived $CO_2$ on reservoirs

Cementation is the most destructive diagenesis in oil and gas reservoirs, and carbonate minerals are the most common types of cement and can negatively impact reservoir properties (Ketzer et al., 2003; Ehrenberg and Baek, 2019). In mantle-derived $CO_2$ gas reservoirs, after a prolonged $CO_2$-water-rock interaction, $CO_2$ gas reservoirs will also precipitate carbonate cement such as dawsonite, calcite, siderite, ankerite, and dolomite (Figures 5A–I, e.g., Ahmat et al., 2022; Worden, 2006; Liu et al., 2009). These minerals will occupy the pore spaces (Figures 5A–I), leading to the deterioration of reservoir quality. There are fair negative correlations between the content of carbonate minerals, porosity, and permeability of mantle-derived $CO_2$ reservoirs (Figures 7A, B), indicating that the cementation of carbonate minerals affected by $CO_2$ is the primary factor leading to the deterioration of $CO_2$ reservoir quality (e.g., Ahmat et al., 2022).

In addition, dawsonite cements are commonly accompanied by authigenic quartz (Figure 5A) (Equations 2–4), and feldspar dissolution can generate authigenic quartz and diverse clay minerals, like kaolinite, I/S (Li et al., 2021). These authigenic quartz fill the pores and reduce the porosity of the reservoirs, while the clay minerals may block the pores and throats and decrease the permeability (Pearce et al., 2019; Wu et al., 2019; Aminu et al., 2018), which can to some extent decrease the quality of the reservoirs.

## 5.3 The impacts of mantle-derived $CO_2$ on reservoirs in different fluid environments

### 5.3.1 The impacts of mantle-derived $CO_2$ on sandstone reservoirs in open fluid environments

In oil and gas fields with faults, reservoirs near faults typically exhibit relatively good reservoir properties and relatively open fluid environments compared to reservoirs far from faults (Gudmundsson, 2022; Wei et al., 2017; Ward et al., 2016). The good reservoir properties are largely attributed to the dissolution effects of organic acids and the timely migration of dissolution by-products facilitated by formation fluids (Wuelstefeld et al., 2017; Zhou et al., 2020; Li et al., 2016). Similarly, the reservoirs near the faults in the study area all have good porosity and permeability (Figure 4; e.g., Hu, 2016; Wei et al., 2017). For example, the well A, located

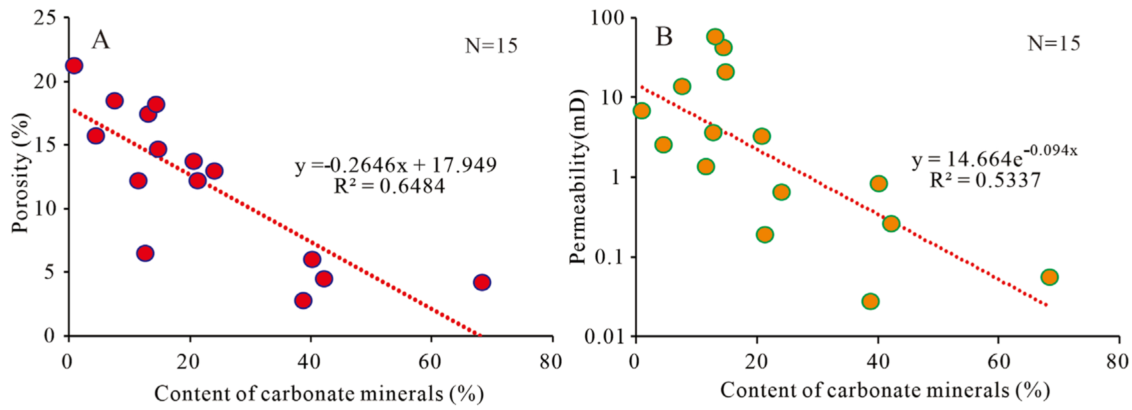


FIGURE 7
The relationship between contents of carbonate minerals and porosity **(A)** and permeability **(B)** in the mantle-derived $CO_2$ reservoirs.

near the fault, has an average porosity of 23.6% and an average permeability of 84.0 mD. According to the curves of average porosity and permeability, the vertical variation between porosity and permeability is relatively small (Figure 8). The dissolution of feldspar and early calcite in the reservoir is extremely intensive (Figure 8). The by-products of dissolution, clay minerals, are few and mainly composed of kaolinite (Figure 3). The carbonate cementation in Well A is weak, with only a small amount of other carbonate cement, except dawsonite that can stably exist in high $CO_2$ concentrations environment (Table 2).

Accordingly, In the open fluid environment near the fault in the study area, the by-products of feldspar dissolution (clay minerals and siliceous cement) are carried out from the reservoir by the flow of formation fluid (e.g., Wuelstefeld et al., 2017; Hu, 2016; Wei et al., 2017). In addition, the high-temperature environment provided by the influx of deep fluids also effectively intensifies the dissolution of feldspars and carbonate minerals (e.g., Wuelstefeld et al., 2017). All of these will lead to a significant improvement in reservoir quality. The abundant presence of kaolinite (Table 2) indicates that the fluid environment is acidic, which can inhibit the carbonate cementation (Boyer, 1983). Therefore, there is only a small amount of carbonate cement in the $CO_2$ reservoirs with open fluid environments (Table 2). Although there may be some dawsonite in high-concentration $CO_2$ environments, it cannot prevent the overall trend of improving reservoir quality (Figure 8).

In summary, an open fluid environment facilitates the dissolution of reservoirs by $CO_2$, facilitating the removal of dissolution products from the reservoirs, and high $CO_2$ concentration inhibits carbonate mineral cementation, greatly increasing reservoir porosity and permeability.

### 5.3.2 The impacts of mantle-derived $CO_2$ on sandstone reservoirs in closed fluid environments

In reservoirs located far from faults, the fluid environment is generally more closed, leading to limited fluid flow and complex diagenesis (Macaulay et al., 2001; Wang et al., 2017; Ahmat, et al., 2022; Yuan et al., 2013b). Clay minerals assemblages were used to identify closed fluid environments (Azzam et al., 2023; Lv et al., 2022). In the study area, the mantle-derived $CO_2$ reservoirs far away from faults have rare plagioclase, massive carbonate minerals, and I/S (Table 2; e.g., Azzam et al., 2023; Lv et al., 2022), which may imply the relatively closed fluid environment and mineral formation process. Initially, $CO_2$ entered the reservoirs to form an acidic environment, causing significant dissolution of plagioclase, generating dissolution pores and massive I/S. However, due to the difficulty of fluid flow in reservoirs far from faults, the dissolution by-products, such as $Na^+$, $Ca^{2+}$, and $Al^{3+}$, were not discharged timely, forming a local alkaline environment. Because I/S cannot be converted into kaolinite in alkaline environments (Yuan et al., 2013b), a large amount of I/S remains in the reservoirs. Meanwhile, the alkaline environments also lead to the precipitation of carbonate minerals in pre-existing dissolution pores (Figures 5C–E; e.g., Macaulay et al., 2001). In addition, reservoirs far from faults generally keep lower $CO_2$ content. For example, the well C is in a low $CO_2$ content area (Figure 1B), which also proves that the fluid environment of $CO_2$ reservoirs in well C is relatively closed.

After mantle-derived $CO_2$ enters the trap, $CO_2$ gradually migrates towards the top of the reservoir by the action of buoyancy (Wei et al., 2023; Gudmundsson, 2022), eventually leading to a decrease in $CO_2$ concentration with increasing depth (Figure 9). The higher the concentration of $CO_2$, the stronger the acidity of the fluid and the more intense the dissolution of reservoirs. Therefore, as the depth increases, the dissolution of the reservoir gradually weakens (Figure 9). The acidity of the fluid can also inhibit the cementation of carbonate minerals (Sun et al., 2020), so the carbonate cementation at the top of the reservoir is relatively weak (Figure 9). The prolonged contact between high concentrations of mantle-derived $CO_2$, formation water, and debris particles leads to strong dissolution of feldspar and early carbonate minerals (Figure 5J–L, e.g., Azzam et al., 2023; Lv et al., 2022), resulting in increased salinity of formation water (Giles and Boer, 1990; Yuan et al., 2013b). Due to the vertical difference of $CO_2$ concentration in the reservoir, the salinity of the formation water

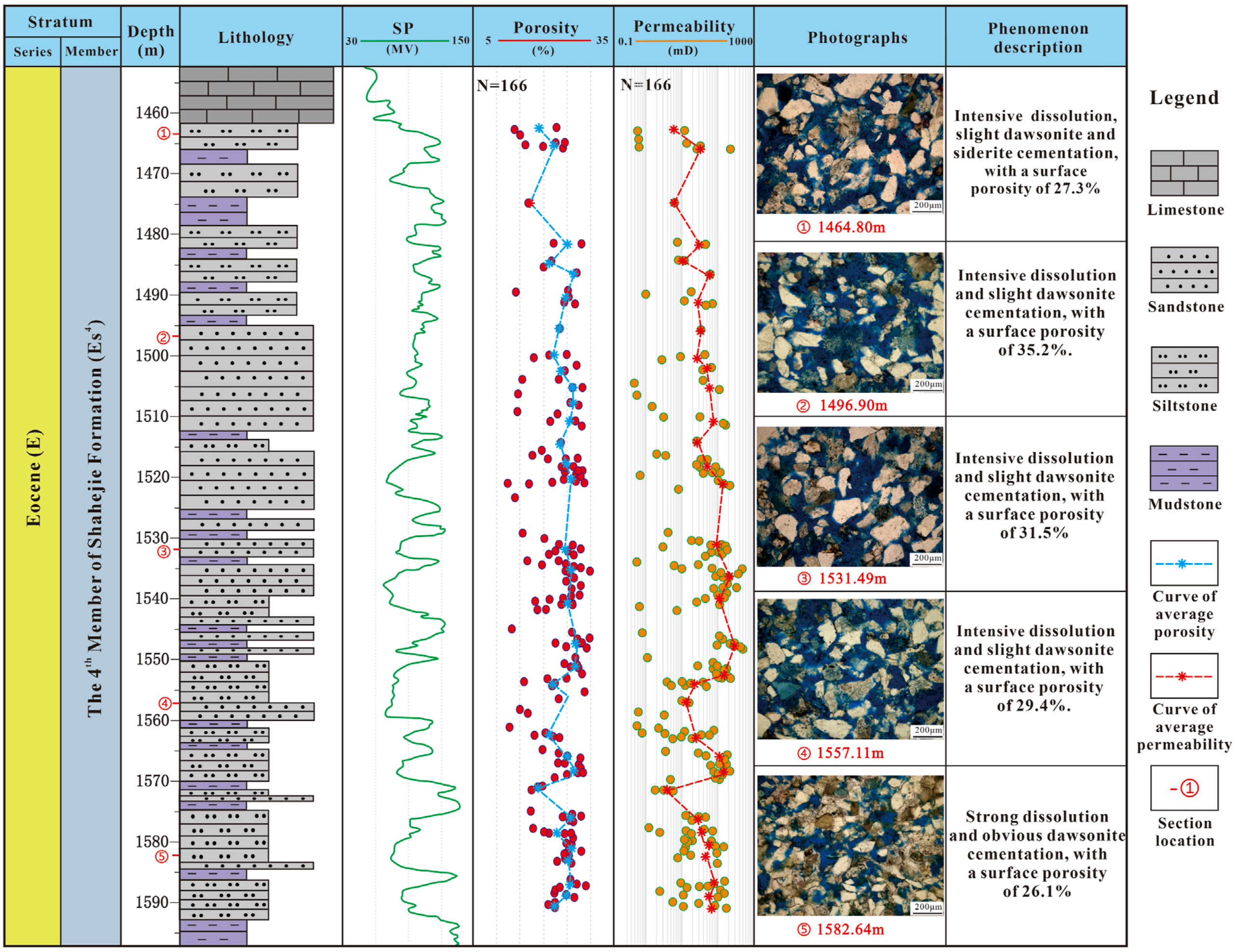


FIGURE 8
Composite columnar section of lithology, porosity, permeability, and diagenesis characteristics of Well A in an open fluid environment.

at the top of the reservoir would be higher than that at the bottom after a long-term $CO_2$-water-rock interaction. Naturally, high salinity formation water and dissolution by-products migrate and diffuse downwards under the influence of the difference in salinity. Therefore, the dissolution products at the top of the reservoir will also migrate downwards and recrystallize. In addition, as the depth increases, the $CO_2$ concentration decreases, the fluid alkalinity increases, and $CO_2$ gradually participates in carbonate minerals cementation (Figure 9).

In summary, within closed fluid environment reservoirs, as depth increases, dissolution gradually weakens while carbonate cementation strengthens (Figure 9). The constructive effects of dissolution and the destructive effects of carbonate cementation work synergistically, resulting in a gradual decrease in porosity and permeability (Figure 7). This trend is observed across each sand layer (Figure 9).

### 5.3.3 Impact pattern of mantle-derived $CO_2$ on reservoirs in open and closed fluid environments

Based on the argument above, a comprehensive pattern of the impact of $CO_2$ on reservoirs within open and closed fluid environments in the study area has been established (Figure 10). The reservoirs near the faults keep an open fluid environment, while the further away from the faults, the more closed the fluid environment is (e.g., Gudmundsson, 2022; Ward et al., 2016; Macaulay et al., 2001; Wang et al., 2017; Ahmat, et al., 2022). As the distance from the fault increases, the dissolution weakens, carbonate cementation strengthens, contents of clay minerals and the relative content of I/S increase, while the relative content of kaolinite decreases (e.g., Azzam et al., 2023; Lv et al., 2022). In an open fluid environment, feldspar strongly dissolves and generates a large number of dissolution pores (e.g., Hu, 2016; Wei and Sun, 2017), and the dissolution by-products (clay minerals) are timely removed from the reservoirs and migrate northward along the faults with the fluids. Moreover, the acidic environment formed by $CO_2$ inhibits the precipitation of carbonate minerals (Boyer, 1983), so there are only a few carbonate cements. All of these effectively improve the physical properties of reservoirs. In a relatively closed fluid environment, as the depth increases, the $CO_2$ concentration decreases, the acidity of the formation water weakens, and the dissolution weakens, but the cementation of carbonate minerals strengthens. Due to the higher $CO_2$ content at the top of the reservoir

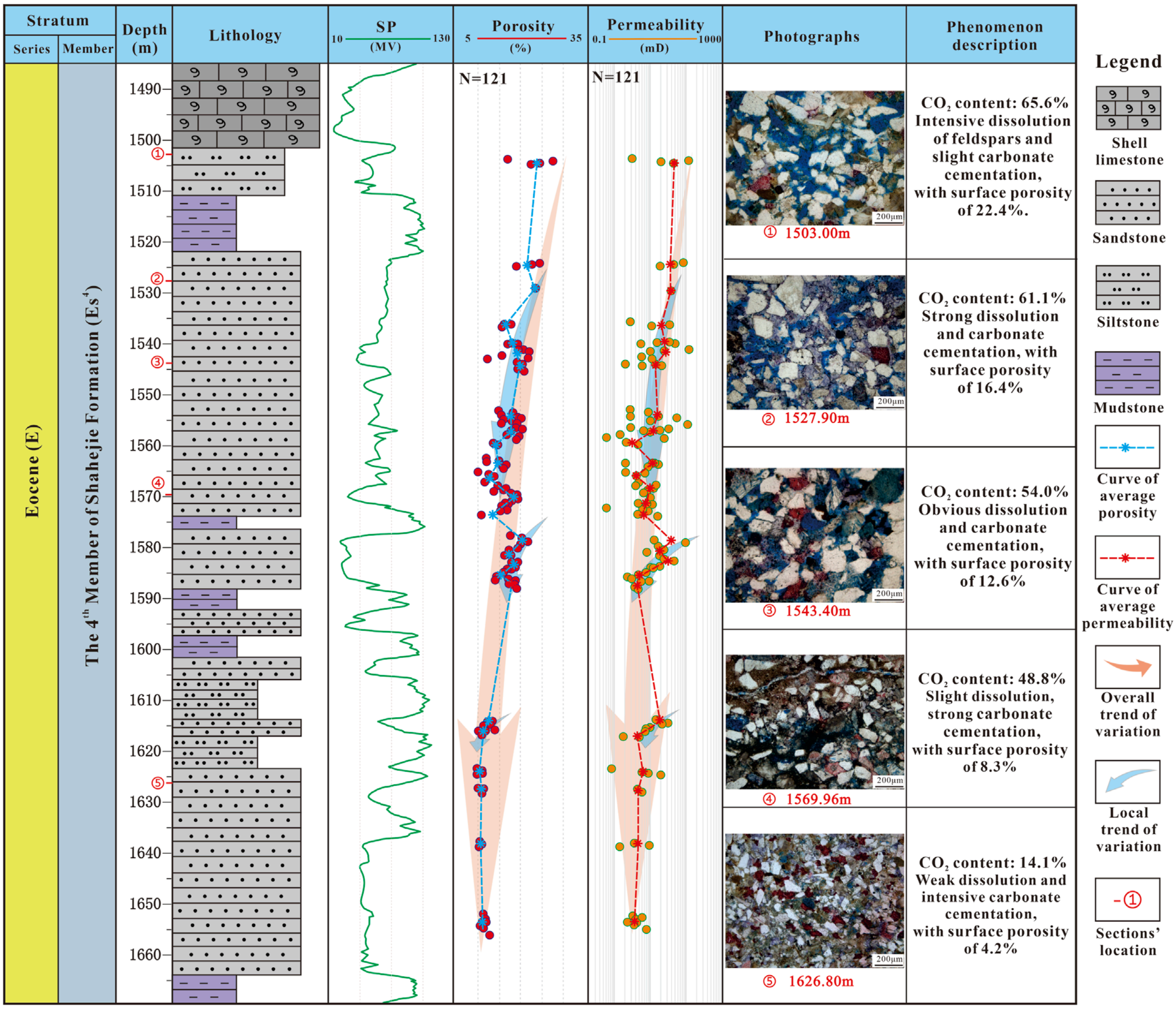


FIGURE 9
Composite columnar section of lithology, porosity, permeability, and diagenesis characteristics of Well C in a relatively closed fluid environment.

compared to the bottom, the $CO_2$-water-rock interactions are more intense, leading to differences in the concentration of dissolution by-products between the upper and lower parts of the reservoirs. Although dissolution products cannot be effectively discharged from the reservoir or transported over long distances (Yuan et al., 2013b), they would migrate downwards and recrystallize due to the concentration gradient of the by-products. Ultimately, the porosity and permeability of reservoirs gradually decrease with depth.

Previous experiments have demonstrated that $CO_2$ primarily participates in mineral dissolution, often overlooking the dual effects of $CO_2$ on reservoirs and the roles of fluid environments in this context under geological conditions. This is why it's important to select geological cases to illustrate the impact of $CO_2$ on reservoirs. This work confirms the influence of mantle-derived $CO_2$ on reservoirs through mineralogy (dawsonite and ankerite) and geochemistry (stable C- and O-isotopes), and further demonstrates the dual effects (dissolution and cementation) of mantle-derived $CO_2$ on reservoirs integrated with reservoir physical properties, with a particular focus on how $CO_2$ influences reservoirs in different fluid environments. However, due to the limitation of $CO_2$ content range (about 15%–70%) in the study area, we are unable to investigate the effects of low-concentration $CO_2$ on sandstone reservoirs, which may affect the generalizability of this study. Besides, the formation temperature and pressure, and salinity of formation water should be considered when dealing with other cases. Overall, this work can be applied to the studies of reservoir homogeneity and sweet spots in regions with hydrothermal and mantle-derived $CO_2$ activities.

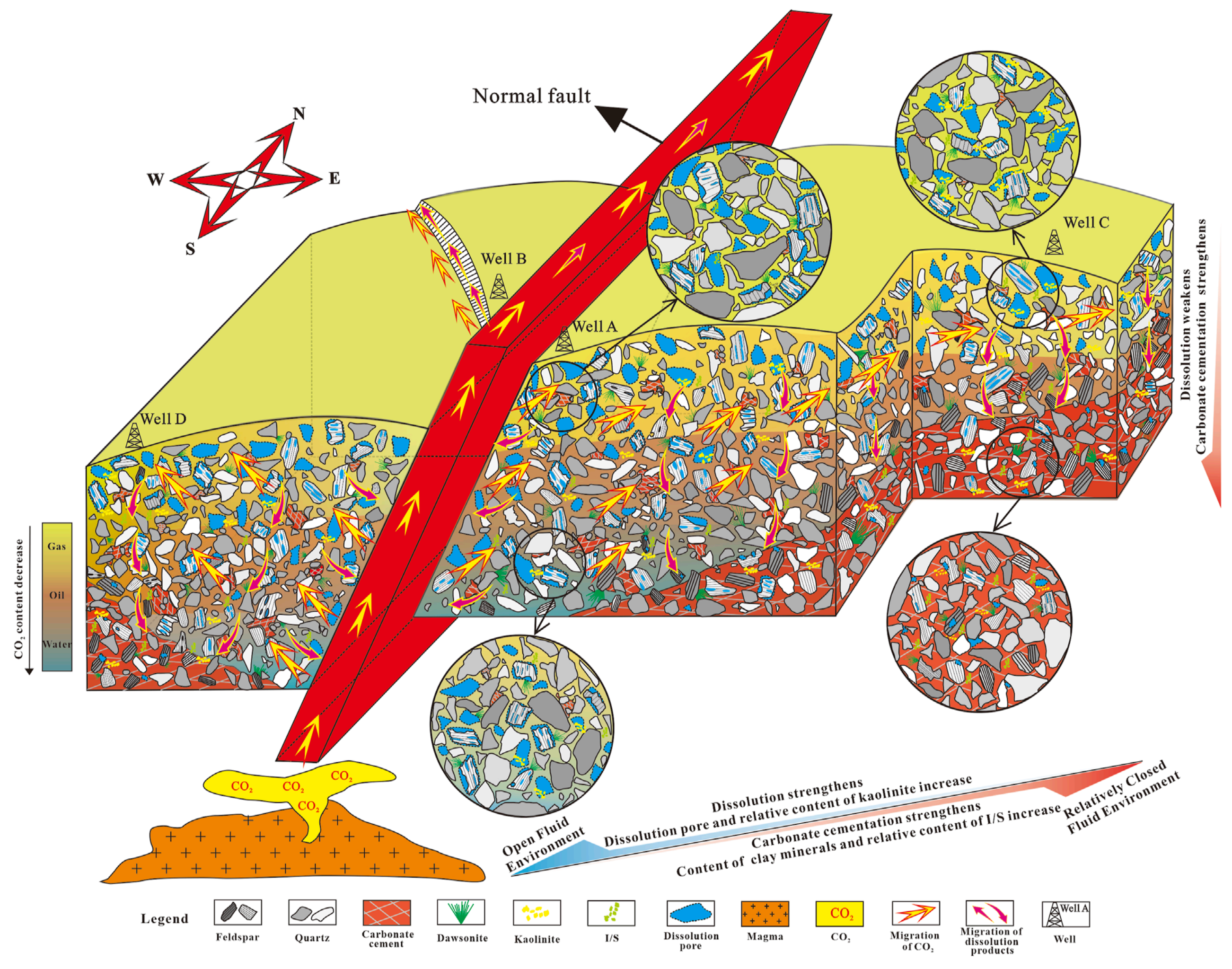


FIGURE 10
The pattern diagram of the impacts of $CO_2$ on reservoirs in open and relatively closed fluid environments.

## 6 Conclusion

In this paper, we take a $CO_2$ gas reservoir in the Dongying Sag, Bohai Bay Basin, China, as an example, using a multi-technique approach in mineralogy and geochemistry to investigate evidence of the impact of mantle-derived $CO_2$ on the reservoir. Combining with the charateristics of the reservoir's physical properties, we elucidate the mechanisms through which mantle-derived $CO_2$ influences the sandstone reservoirs and discuss the patterns of its impact on reservoir properties in open and closed fluid environments. The conclusions can be drawn as follows:

(1) Dawsonite (a special tracer mineral of mantle-derived $CO_2$) and ankerite (its crystallization temperature is much higher than the normal geothermal gradient of the study area) are widely distributed in the $CO_2$ reservoir of the Dongying Sag. Moreover, the $\delta^{13}C$ (−9.0‰–−1.6‰) and $\delta^{18}O$ (−21.7–−12.7‰) of carbonate cements in the mantle-derived $CO_2$ gas reservoir basically fall within the range suggested for mantle-derived $CO_2$ and hydrothermal fluids. These mineralogical and geochemical evidence indicate that $CO_2$-rich hydrothermal fluids have actively participated in water-rock reactions within the reservoir, thereby impacting its diagenesis.

(2) The $CO_2$ reservoirs near faults in the study area are an open fluid environment, while the $CO_2$ reservoirs far from faults keep a relatively closed fluid environment. There are significant differences in the debris particles, mineral composition, and physical properties between reservoirs in open fluid environments and closed fluid environments. The former has better porosity and permeability, more quartz, as well as fewer feldspar, carbonate, and clay mineral cement. Furthermore, the clay minerals in open fluid environments are predominantly kaolinite, whereas these in closed fluid environments primarily consist of I/S.

(3) The mantle-derived $CO_2$ has dual effects on sandstone reservoirs. On the one hand, the dissolution by $CO_2$ greatly increases the reservoir's storage and seepage capacity. On the other hand, the carbonate cement formed by the $CO_2$-water-rock reaction can also lead to serious deterioration of

reservoir quality. In open fluid environments, $CO_2$ strongly dissolves feldspar and carbonate minerals in reservoirs, and the dissolution by-products (clay minerals) are carried out from the reservoirs timely, and the acidic environment formed by $CO_2$ inhibits carbonate cementation, which synergistically improves the physical properties of reservoirs. In closed fluid environments, decreasing $CO_2$ concentrations with depth leads to diminishing dissolution effects and increased carbonate cementation, resulting in reduced reservoir porosity and permeability.

However, the $CO_2$ content, the formation temperature and pressure, and salinity of formation water should be considered when dealing with other cases. Overall, this study provides a good understanding for the impacts of mantle-derived $CO_2$ on sandstone diagenesis and reservoir properties in open and closed fluid environments, which may contribute to the studies of reservoir homogeneity and sweet spots in regions with hydrothermal and mantle-derived $CO_2$ activities.

## Data availability statement

The original contributions presented in the study are included in the article/supplementary material, further inquiries can be directed to the corresponding authors.

## Author contributions

MW: Conceptualization, Investigation, Methodology, Writing–original draft, Writing–review and editing. JZ: Project administration, Resources, Supervision, Writing–review and editing. CL: Writing–review and editing, Investigation. JQ: Supervision, Validation, Writing–review and editing. WW: Investigation, Writing–original draft. HZ: Investigation, Writing–review and editing. HC: Investigation, Writing–review and editing.

## Funding

The author(s) declare that financial support was received for the research, authorship, and/or publication of this article. This work is supported by the National Natural Science Foundation of China, Grant number 42302144.

## Acknowledgments

We would like to express our sincere gratitude to the Petroleum Exploration and Development Research Institute of Shengli Oilfield, China Petroleum and Chemical Corporation, for providing us with the core samples and data used in this study. Additionally, we would like to extend our special thanks to the reviewers and editors for their insightful comments and suggestions, which have greatly helped to improve the quality of this article.

## Conflict of interest

The authors declare that the research was conducted in the absence of any commercial or financial relationships that could be construed as a potential conflict of interest.

## Publisher's note

All claims expressed in this article are solely those of the authors and do not necessarily represent those of their affiliated organizations, or those of the publisher, the editors and the reviewers. Any product that may be evaluated in this article, or claim that may be made by its manufacturer, is not guaranteed or endorsed by the publisher.

## References

Ahmat, K., Cheng, J., Yu, Y., Zhao, R., and Li, R. (2022). $CO_2$-water-rock interactions in carbonate formations at the tazhong uplift, Tarim basin, China. *Minerals* 12, 635. doi:10.3390/min12050635

Aminu, D. M., Nabavi, A. S., and Manovic, V. (2018). $CO_2$-brine-rock interactions: the effect of impurities on grain size distribution and reservoir permeability. *Int. J. Greenh. Gas Control* 78, 168–176. doi:10.1016/j.ijggc.2018.08.008

Anderson, C. D. S., Gabriella, D. O. Q., Julio, C. M., João, M., Mauro, C. G., Fred, J., et al. (2023). Petrogenetic insights on tephritic magmatism from davis bank South Atlantic ocean-vitória-trindade ridge VTR, Brazil: the role of a $CO_2$-enriched mantle source. *J. S. Am. Earth Sci.* 122, 104170. doi:10.1016/j.jsames.2022.104170

Azzam, F., Blaise, T., Dewla, M., Patrier, P., Beaufort, D., Abd Elmola, A., et al. (2023). Role of depositional environment on clay coat distribution in deeply buried turbidite sandstones: insights from the agat field, Norwegian North Sea. *Mar. Petroleum Geol.* 155, 106379. doi:10.1016/j.marpetgeo.2023.106379

Boyer, F. (1983). *Depositional environments and diagenetic history of the springer formation: ardmore basin, Oklahoma*. Dallas: The University of Texas at.

Cheng, X., Cao, Y., Yuan, G., Wang, Y., and Zan, N. (2020). Origin and distribution model of the lower Paleozoic carbonate reservoirs in pingfangwang pingnan buried hills, Dongying Sag. *J. China Univ. Petroleum Ed. Nat. Sci.* 44, 1–14. doi:10.13969/j.issn.1673-5005.2020.03.001

Dai, J., Shi, X., and Wei, Y. (2001). Summary of the abiogenic origin theory and the abiogenic gas pools (fields). *Acta Pet. Si-Nica* 22, 5–10.

Diker, C., Ulusoy, İ., Akkaş, E., Aydın, E., Gümüş, E., Gümüş, E., et al. (2024). Hydrothermal fluid circulation within the restless structural frame of Hasandağ volcanic system (Central Anatolia, Türkiye) inferred from self-potential, $CO_2$, and temperature measurements. *J. Volcanol. Geotherm. Res.* 446, 107994. doi:10.1016/J.JVOLGEORES.2023.107994

Dmitriyevskiy, N. A., Kireyev, A. F., Bochko, A. R., and Fedorova, T. A. (2010). Hydrothermal origin of oil and gas reservoirs in basement rock of the southern vietnam continental shelf. *Int. Geol. Rev.* 35 (7), 621–630. doi:10.1080/00206819309465547

Ehrenberg, S. N., and Baek, H. (2019). Deposition, diagenesis and reservoir quality of an oligocene reefal-margin limestone succession: asmari formation, United Arab Emirates. *Sediment. Geol.* 393, 105535. doi:10.1016/j.sedgeo.2019.105535

Ewa, S., Hervé, M., Morihisa, H., Michał, Ś., Andrzej, D., Jens, G., et al. (2012). Evidence in archaean alkali feldspar megacrysts for high-temperature interaction with mantle fluids. *J. Petrology* 53, 67–98. doi:10.1093/petrology/egr056

Fischer, S., Axel, L., and Maren, W. (2010). $CO_2$-brine-rock interaction - first results of long-term exposure experiments at *in situ* P-T conditions of the ketzin $CO_2$ reservoir. *Chem. Erde* 70, 155–164. doi:10.1016/j.chemer.2010.06.001

Folk, R. L. (1968). *The petrology of sedimentary rocks*. Austin, Texas: Hemphill Publishing Company, 127.

Friedman, N., and O'Neil, J. R. (1977). *Data of geochemistry: compilation of stable isotope fractionation factors of geochemical interest*. Washington: D.C: US Government Printing Office.

Fu, M., Song, R., Xie, Y., Zhang, S. n., Gluyas, J. G., Zhang, Y. z., et al. (2016). Diagenesis and reservoir quality of overpressured deep-water sandstone following inorganic carbon dioxide accumulation: upper miocene huangliu formation, Yinggehai Basin, South China Sea. *Mar. Petroleum Geol.* 77, 954–972. doi:10.1016/j.marpetgeo.2016.08.005

Giles, M. R., and de Boer, R. B. (1990). Origin and significance of redistributional secondary porosity. *Mar. Petroleum Geol.* 7, 378–397. doi:10.1016/0264-8172(90)90016-a

Gong, J., Zhang, J., Zhang, S., and Zhang, L. (2013). The effect of the Paleogene-Neogene magmation on hydrocarbon-generating region of the upper $Es_{3-4}$-middle $Es_3$ dark argillaceous rocks in Dongying Depression. *J. Northwest Univ. Nat. Sci. Ed.* 43, 101–108. doi:10.16152/j.cnki.xdxbzr.2013.01.016

Gudmundsson, S. (2022). Transport of geothermal fluids along dikes and fault zones. *Energies* 15, 7106. doi:10.3390/en15197106

Guo, D., Xia, B., Wang, X., and Zhang, S. (2006). Relationship between faulting and reservoiring of $CO_2$ in jiyang depression. *Nat. Gas. Ind.* 26, 40–42.

Guo, X., He, S., Liu, K., Cao, F., Shi, H., and Zhu, J. (2011). Condensates in the PY30-I structure, Panyu uplift, Pearl River Mouth basin, South China Sea: evidence for hydrothermal activity associated with petroleum migration and accumulation. *J. Petroleum Geol.* 34 (2), 217–232. doi:10.1111/j.1747-5457.2011.00502.x

Han, H., Zhang, J., Zhang, J., Wu, H., Xiang, X., and Lei, Y. (2010). A study on the phase of $CO_2$ pools underground, Jiyang depression. *J. Northwest Univ. Nat. Sci. Ed.* 40, 493–496. doi:10.16152/j.cnki.xdxbzr.2010.03.020

Han, Y., He, S., Song, G., Wang, Y., Hao, X., Wang, B., et al. (2012). Origin of carbonate cement in the overpressured top seal and adjacent sandstones in Dongying Depression. *Acta Pet. Sin.* 33, 385–393.

Harrison, A. L., Tutolo, B. M., and DePaolo, D. J. (2019). The role of reactive transport modeling in geologic carbon storage. *Int. Mag. Mineralogy, Geochem. Petrology* 15, 93–98. doi:10.2138/gselements.15.2.93

Hou, Z., Chen, S., Liu, H., Yang, H., and Wang, Y. (2019). Hydrothermal fluid activity and its hydrocarbon geological significance in Dongying Depression. *J. China Univ. Min. and Technol.* 48, 1090–1101. doi:10.13247/j.cnki.jcumt.000999

Hu, W. (2016). Origin and Indicators of deep-seated fluids in sedimentary basins. *Bull. Mineralogy, Petrology Geochem.* 35, 817–826. doi:10.3969/j.issn.1007-2802.2016.05.002

Huang, X., Jin, Z., Liu, Q., Meng, Q., Zhu, D., Liu, J., et al. (2021). Catalytic hydrogenation of post-Mature hydrocarbon source rocks under deep-derived fluids: an example of early Cambrian Yurtus formation, Tarim basin, NW China. *Front. Earth Sci.* 9. doi:10.3389/FEART.2021.626111

Jin, Z., Zhu, D., Meng, Q., and Hu, W. (2013). Hydrothermal activities and influences on migration of oil and gas in Tarim Basin. *Acta Petrol. Sin.* 29, 1048–1058.

Johnson, G., Nightingale, B. M., Shevalier, M., and Hutcheon, I. (2011). Using oxygen isotope ratios to quantitatively assess trapping mechanisms during $CO_2$ injection into geological reservoirs: the pembina case study. *Chem. Geol.* 283, 185–193. doi:10.1016/j.chemgeo.2011.01.016

Kang, Y., Zou, L., Liu, Z., Han, M., Lu, H., and Yao, S. (2014). Faulted structure and its effect on oil–gas reservoir forming in Qingcheng arch. *Petroleum Geol. Recovery Effic.* 21, 45–48. doi:10.13673/j.cnki.cn37-1359/te.2014.06.011

Ketzer, J. M., Holz, M., Morad, S., and Al-Aasm, J. S. (2003). Sequence stratigraphic distribution of diagenetic alterations in coal-bearing, paralic sandstones: evidence from the rio bonito formation (early permian), southern Brazil. *Sedimentology* 50 (5), 855–877. doi:10.1046/j.1365-3091.2003.00586.x

Li, J., Li, H., Jiang, W., Cai, M. L., He, J., Wang, Q., et al. (2024). Shale pore characteristics and their impact on the gas-bearing properties of the Longmaxi Formation in the Luzhou area. *Sci. Rep.* 14, 16896. doi:10.1038/s41598-024-66759-7

Li, L., Zhong, D., Yang, C., and Zhao, L. (2016). Faults role in formation and distribution of the mantle derived carbon dioxide gas pools: case study of the Jiyang depression in Bohai Bay Basin, China. *Acta Petrol. Sin.* 32, 2209–2216.

Li, M., Song, L., Yu, H., Cao, Y., and Yuan, G. (2021). Influence of pH value on feldspar dissolution and pore-increasing effect. *J. China Univ. Petroleum Ed. Nat. Sci.* 45, 33–41. doi:10.3969/j.issn.1673-5005.2021.05.004

Li, Z., Guo, J., Zhang, Y., and Chen, J. (2015). High–temperature supercritical $CO_2$ water-rock simulation experiment of sandstone and its geological significance. *Nat. Gas. Ind.* 35, 31–38. doi:10.3787/j.issn.1000-0976.2015.05.0075

Liu, H., Liu, C., Zhang, H., Zhou, Z., and Han, F. (2024). The precipitation mechanisms of scheelite from $CO_2$-rich hydrothermal fluids: Insight from thermodynamic modeling. *Appl. Geochem.* 175, 106187. doi:10.1016/J.APGEOCHEM.2024.106187

Liu, J., Ge, Z., and Li, X. (2023). The accumulation law and helium-rich genesis of $CO_2$ gas reservoir in Subei Basin. *Nat. Gas. Geosci.* 34, 477–485. doi:10.11764/j.issn.1672-1926.2022.11.005

Liu, J., Pujol, M., Zhou, H., Selby, D., Li, J., and Cheng, B. (2022). Origin and evolution of a $CO_2$-Rich gas reservoir offshore Angola: insights from the gas composition and isotope analysis. *Appl. Geochem.* 148, 105552. doi:10.1016/j.apgeochem.2022.105552

Liu, L., Ming, X., Liu, N., Yang, H., Yu, L., Bai, H., et al. (2016). Characteristics and formation mechanism of Muti-layer distribution of dawsonite in the Honggang oil field, southern Songliao Basin. *Bull. Mineralogy, Petrology Geochem.* 35, 817–826. doi:10.3969/j.issn.1007-2802.2016.05.007

Liu, L., Zhu, D., Qu, Z., Jin, Z., Wang, X., and Dong, L. (2009). Impacts of mantle–genetic $CO_2$ influx on the reservoir quality of lower cretaceous sandstone from wuerxun depression, Hailaer Basin. *Acta Petrol. Sin.* 25, 2311–2319.

Liu, N., Wu, K., Liu, L., Yu, L., and Sun, Y. (2019). Dawsonite characteristics and its implications on the $CO_2$ in Yinggehai-Huangliu formation of Ledong area, Yinggehai Basin. *Earth Sci.* 44, 2695–2703. doi:10.3799/dqkx.2019.106

Liu, Q., Wu, X., Wang, X., Jin, Z., Zhu, D., Meng, Q., et al. (2019). Carbon and hydrogen isotopes of methane, ethane, and propane: a review of genetic identification of natural gas. *Earth-Science Rev.* 190, 247–272. doi:10.1016/j.earscirev.2018.11.017

Liu, Q., Zhu, D., Jin, Z., Meng, Q., and Yu, H. (2017). Effects of deep $CO_2$ on petroleum and thermal alteration: the case of the Huangqiao oil and gas field. *Chem. Geol.* 469, 214–229. doi:10.1016/j.chemgeo.2017.06.031

Liu, Q., Zhu, D., Jin, Z., Tian, H., Zhou, B., Jiang, P., et al. (2023). Carbon capture and storage for long-term and safe sealing with constrained natural $CO_2$ analogs. *Renew. Sustain. Energy Rev.* 17, 113000. doi:10.1016/J.RSER.2022.113000

Liu, R., Heinemann, N., Liu, J., Zhu, W., Wilkinson, M., Xie, Y., et al. (2019). $CO_2$ sequestration by mineral trapping in natural analogues in the Yinggehai Basin, South China Sea. *Mar. Petroleum Geol.* 104, 190–199. doi:10.1016/j.marpetgeo.2019.03.018

Lu, J., Li, C., Wang, M., and Zhang, C. (2022). Review of deep fluids in sedimentary basins and their influence on resources, with a focus on oil and geothermal exploitation. *Front. Earth Sci.* 10. doi:10.3389/feart.2022.896629

Lv, X., Fu, M., Zhang, S., Meng, X., Liu, Y., Ding, X., et al. (2022). Effect of diagenesis on the quality of sandstone reservoirs Exposed to high-temperature, overpressure, and $CO_2$-Charging conditions: a case study of upper Miocene Huangliu sandstones of Dongfang District, Yinggehai Basin, South China Sea. *Front. Earth Sci.* 10. doi:10.3389/feart.2022.885602

Ma, P., Lin, C., Zhang, S., Dong, C., Zhao, Y., Dong, D., et al. (2018). Diagenetic history and reservoir quality of tight sandstones: a case study from Shiqianfeng sandstones in upper Permian of Dongpu Depression, Bohai Bay Basin, eastern China. *Mar. Petroleum Geol.* 89, 280–299. doi:10.1016/j.marpetgeo.2017.09.029

Macaulay, C. I., Beckett, D., Beckett, D., Braithwaite, K., Bliefnick, D., and Philps, B. (2001). Constraints on diagenesis and reservoir quality in the fractured hasdrubal field, offshore Tunisia. *J. Petroleum Geol.* 24 (1), 55–78. doi:10.1111/j.1747-5457.2001.tb00661.x

Miao, Q., Xu, C., Hao, F., Yin, J., Wang, Q., Xie, M., et al. (2020). Roles of fault structures on the distribution of mantle-derived $CO_2$ in the Bohai Bay Basin, NE China. *J. Asian Earth Sci.* 197, 104398. doi:10.1016/j.jseaes.2020.104398

Morishita, Y. (2023). Hydrothermal calcite precipitation in veins: Inspired by experiments for oxygen isotope fractionation between $CO_2$ and calcite from 1°C to 150°C. *Appl. Sci.* 13 (9), 5610. doi:10.3390/app13095610

Niu, Z., Wang, Y., Wang, X., Meng, W., Liu, X., Wang, R., et al. (2022). Characteristics of crude oil with different sulfur content and genesis analysis of high-sulfur crude oil in the eastern section of the southern slope of Dongying Sag. *Petroleum Geol. Recovery Effic.* 19, 15–27. doi:10.13673/j.cnki.cn37-1359/te.202108024

Oluwadebi, A. g., Taylor, K. G., and Dowwey, P. J. (2018). Diagenetic controls on the reservoir quality of the tight gas Collyhurst sandstone formation, lower Permian, East Irish sea basin, United Kingdom. *Sidementary Geol.* 371, 55–74. doi:10.1016/j.sedgeo.2018.04.006

Pearce, J. K., Dawson, G. K. W., Sommacal, S., and Golding, S. D. (2019). Experimental and modelled reactions of $CO_2$ and $SO_2$ with core from a low salinity aquifer overlying a target $CO_2$ storage complex. *Geosciences* 9, 513. doi:10.3390/geosciences9120513

Portier, S., and Rochelle, C. (2005). Modeling $CO_2$ solubility in pure water and NaCl-type waters from 0 to 300°C and from 1 to 300 bar application to the utsira formation at sleipner. *Chem. Geol.* 217, 187–199. doi:10.1016/j.chemgeo.2004.12.007

Ranta, E., Halldórsson, S. A., Barry, P. H., Ono, S., Robin, J. G., Kleine, B. I., et al. (2023). Deep magma degassing and volatile fluxes through volcanic hydrothermal systems: insights from the askja and kverkfjöll volcanoes, Iceland. *J. Volcanol. Geotherm. Res.* 436, 107776. doi:10.1016/j.jvolgeores.2023.107776

Ryzhenko, B. N. (2006). Genesis of dawsonite mineralization: thermodynamic analysis and alternatives. *Geochem. Int.* 44, 835–840. doi:10.1134/S0016702906080088

Sun, C., and Dasgupta, R. (2023). Carbon budget of earth's deep mantle constrained by petrogenesis of silica-poor ocean island basalt. *Earth Planet. Sci. Lett.* 611, 1–12. doi:10.1016/j.epsl.2023.118135

Sun, D., Li, W., Lu, S., Liu, X., He, T., Zhu, P., et al. (2020). Reservoir characteristics and controlling factors of shushanhe formation in yingmaili area of tabei uplift. *J. Northeast Petroleum Univ.* 44, 82–93. doi:10.3969/j.issn.2095-4107.2020.06.009

Wang, D., and Zhang, Y. (2001). A study on the origin of the carbonate cement within the reservoir in the external metamorphic belt of the Bohai Bay oil–gas bearing region. *Petroleum Explor. Dev.* 28, 40–42.

Wang, J., Cao, Y., Song, G., and Liu, H. (2017). Diagenetic evolution and formation mechanisms of high-quality reservoirs under multiple diagenetic environmental constraints: an example from the paleogene beach-bar sandstone reservoirs in the dongying depression, Bohai Bay Basin. *Acta Geol. Sin.* 91, 232–248. doi:10.1111/1755-6724.13074

Wang, X., Qiu, L., and Jiang, Z. (2004). The relativity of igneous activity and $CO_2$ gas reservoir in jiyang depression. *Nat. Gas. Geosci.* 15, 422–427.

Ward, N. I. P., Alves, T. M., and Blenkisop, T. G. (2016). Reservoir leakage along concentric faults in the southern north Sea: implications for the deployment of CCS and EOR techniques. *Toctonophysics* 690, 97–116. doi:10.1016/j.tecto.2016.07.027

Wei, W., Zhu, X., Lu, P., and Tan, M. (2023). Effects of inorganic $CO_2$ intrusion on diagenesis and reservoir quality of lacustrine conglomerate sandstones: implications for geological carbon sequestration. *Geoenergy Sci. Eng.* 229, 212111–212280. doi:10.1016/j.geoen.2023.212111

Wei, W., Zhu, X., Tan, M., Wu, C., Xue, M., Guo, D., et al. (2017). The early cretaceous thermal fluid activities and their impacts on clastic reservoir rocks in the bayingebei formation of chagan sag. *Oil and Gas Geol.* 38, 270–280. doi:10.11743/ogg20170207

Wei, X., and Sun, Y. (2017). Fault characteristics and controlling factors of hydrocarbon accumulation in qingxi area of dongying depression. *Fault-Block Oil and Gas Field* 4, 154–158. doi:10.6056/dkyqt201702004

Worden, R. H. (2006). Dawsonite cement in the triassic lam formation, shabwa basin, yemen: a natural analog for a potential mineral product of subsurface $CO_2$ storage for greenhouse gas reduction. *Mar. Petroleum Geol.* 23, 61–77. doi:10.1016/j.marpetgeo.2005.07.001

Wright, V. P. (2020). The mantle, $CO_2$ and the giant aptian chemogenic lacustrine carbonate factory of the South Atlantic: some carbonates are made, not born. *Sedimentology* 69, 47–73. doi:10.1111/sed.12835

Wu, S., Zou, C., Ma, D., Zhai, X., Yu, H., and Yu, Z. (2019). Reservoir property changes during $CO_2$ –brine flow through experiments in tight sandstone: implications for $CO_2$ enhanced oil recovery in the triassic chang 7 member tight sandstone, Ordos Basin, China. *J. Asian Earth Sci.* 179, 200–210. doi:10.1016/j.jseaes.2019.05.002

Wuelstefeld, P., Hilse, U., Koehrer, B., Adelmann, D., and Hilgers, C. (2017). Critical evaluation of an upper carboniferous tight gas sandstone reservoir analog: diagenesis and petrophysical aspects. *Mar. Petroleum Geol.* 86, 689–710. doi:10.1016/j.marpetgeo.2017.05.034

Yang, C., Liu, Q., Zhou, Q., et al. (2009). Genetic identification of natural gases in qingshen gas field, Songliao Basin. *Earth Science-Journal China Univ. Geosciences* 34, 792–798.

Yang, J., Qi, N., Ireland, M., Lu, S., Wang, M., Lu, M., et al. (2021). Geological controls on the natural $CO_2$ accumulation in the surennuoer oilfield of the hailar basin, China. *Mar. Petroleum Geol.* 133, 105319. doi:10.1016/j.marpetgeo.2021.105319

Yang, K., He, S., Yang, C., Wang, M., Zhang, R., Ren, S., et al. (2023). Diagenesis characteristics of tight sandstone reservoirs with high temperature, overpressure, and high $CO_2$ content: a case study of neogene meishan-huangliu formation in LD10 area, Yinggehai Basin. *Lithol. Reserv.* 35, 83–95. doi:10.12108/yxyqc.20230108

Yu, M., Liu, L., Yang, S., Yu, Z., Li, S., Yang, Y., et al. (2016). Experimental identification of $CO_2$-oil-brine-rock interactions: implications for $CO_2$ sequestration after termination of a $CO_2$-EOR project. *Appl. Geochem.* 75, 137–151. doi:10.1016/j.apgeochem.2016.10.018

Yuan, G., Cao, Y., Xi, K., Wang, Y., Li, X., and Yang, T. (2013b). Feldspar dissolution and its impact on physical properties of Paleogene clastic reservoirs in the northern slope zone of the Dongying Sag. *Acta Pet. Sin.* 34, 853–866. doi:10.7623/syxb201305006

Yuan, G., Cao, Y., Yang, T., Wang, Y., Li, X., Xi, K., et al. (2013a). Porosity enhancement potential through mineral dissolution by organic acids in the diagenetic process of the clastic reservoir. *Earth Sci. Front.* 20, 207–219.

Yuan, J., Zhou, T., and Zhao, G. (2023). Identification marks of deep thermal fluid activity and its effect on reservoir transformation. *Acta Geol. Sin.* 97, 2067–2083. doi:10.19762/j.cnki.dizhixuebao.2023235

Zeng, J. (2000). Thermal fluid activities and their effects on water-rock interaction in Dongying Sag. *Earth Science-Journal China Univ. Geoscience.* 25, 133–136.

Zhang, C., Liu, D., Liu, Q., Jiang, S., Wang, X., Wang, Y., et al. (2023). Magmatism and hydrocarbon accumulation in sedimentary basins: a review. *Earth-Science Rev.* 244, 104531. doi:10.1016/j.earscirev.2023.104531

Zhang, Y., Hu, W., Yao, S., Yu, H., Kang, X., Wu, H., et al. (2018). The interaction of $CO_2$-rich fluid with sandstone and its significance for sandstone reservoirs of Permian Longtan Formation in Huangqiao area, Subei Basin. *Geol. Bull. China* 37, 1944–1955.

Zhao, F., Jiang, S., Li, S., Cao, W., Wang, G., Zhang, H., et al. (2017). Correlation of inorganic $CO_2$ reservoirs in East China to subduction of paleo-pacific plate. *Earth Sci. Front.* 24, 370–384. doi:10.13745/j.esf.yx.2017-3-12

Zhao, J., Cao, Q., Bai, Y., Er, C., Li, J., Wu, W., et al. (2016). Petroleum accumulation from continuous to discontinuous: concept, classification, and distribution. *Acta Pet. Sin.* 37, 145–159. doi:10.7623/syxb201602001

Zhou, B., Jin, Z., Liu, V., Lun, Z., Meng, Q., and Zhu, D. (2020). Alteration of reservoir-caprock systems by using $CO_2$-rich fluid in the huangqiao area, North Jiangsu Basin. *Oil and Gas Geol.* 41, 1151–1161. doi:10.11743/ogg20200604

Zhu, D., Liu, Q., Jin, Z., Meng, Q., and Hu, W. (2017). Effects of deep fluids on hydrocarbon generation and accumulation in Chinese petroliferous basins. *Acta Geol. Sin. Engl. Ed.* 91, 301–319. doi:10.1111/1755-6724.13079